The Astrophysical Journal, 730:7 (15pp), 2011 March 20 doi:10.1088/0004-637X/730/1/7

BLACK HOLE MASS AND GROWTH RATE AT $z \simeq 4.8$: A SHORT EPISODE OF FAST GROWTH FOLLOWED BY SHORT DUTY CYCLE ACTIVITY*

Benny Trakhtenbrot[1], Hagai Netzer[1], Paulina Lira[2], and Ohad Shemmer[3]
[1] School of Physics and Astronomy and the Wise Observatory, The Raymond and Beverly Sackler Faculty of Exact Sciences, Tel-Aviv University, Tel-Aviv 69978, Israel; trakht@wise.tau.ac.il
[2] Departamento de Astronomía, Universidad de Chile, Camino del Observatorio 1515, Santiago, Chile
[3] Department of Physics, University of North Texas, Denton, TX 76203, USA
Received 2010 September 15; accepted 2010 December 10; published 2011 February 24

ABSTRACT

We present new *H*-band spectroscopy for a flux-limited sample of 40 $z \simeq 4.8$ active galactic nuclei, selected from the Sloan Digital Sky Survey. The sample probably contains the most massive active black holes (BHs) at this redshift and spans a broad range in bolometric luminosity, $2.7 \times 10^{46}\,\mathrm{erg\,s^{-1}} < L_{\rm bol} < 2.4 \times 10^{47}\,\mathrm{erg\,s^{-1}}$. The high-quality observations and the accurate fitting of the Mg II λ2798 line enable us to study, systematically, the distribution of BH mass ($M_{\rm BH}$) and normalized accretion rate ($L/L_{\rm Edd}$) at $z \simeq 4.8$. We find that $10^8\,M_\odot \lesssim M_{\rm BH} \lesssim 6.6 \times 10^9\,M_\odot$ with a median of $\sim 8.4 \times 10^8\,M_\odot$. We also find that $0.2 \lesssim L/L_{\rm Edd} \lesssim 3.9$ with a median of $\sim$0.6. Most of these sources had enough time to grow to their observed mass at $z \simeq 4.8$ from $z = 20$, assuming a range of seed BH masses, with $\sim$40% that are small enough to be stellar remnants. Compared to previously studied samples at $z \simeq 2.4$ and $\simeq$3.3, the masses of the $z \simeq 4.8$ BHs are typically lower by $\sim$0.5 dex and their $L/L_{\rm Edd}$ is higher by a similar factor. The new $z \simeq 4.8$ sample can be considered as the progenitor population of the most massive BHs at $z \simeq 2.4$ and $\simeq$3.3. Such an evolutionary interpretation requires that the growth of the BHs from $z \simeq 4.8$ to $z \simeq 3.3$ and $z \simeq 2.4$ proceeds with short duty cycles, of about 10%–20%, depending on the particular growth scenario.

Key words: galaxies: active – galaxies: nuclei – quasars: emission lines

Online-only material: color figures

1. INTRODUCTION

The local universe provides ample evidence for the existence of supermassive black holes (SMBHs) in the centers of most galaxies. Typical masses are in the range $M_{\rm BH} \sim 10^6$–$10^9\,M_\odot$, with few exceptionally massive objects reaching $\sim 10^{10}\,M_\odot$. As first argued by Soltan (1982), the total local black hole (BH) mass is consistent with the total radiation emitted by accreting SMBHs in active galactic nuclei (AGNs). The accumulation of mass onto SMBHs can be traced back through cosmic history by analyzing the redshift-dependent quasar luminosity function. Such studies suggest that the peak epoch of SMBH growth was at $z \sim 2$–3 (e.g., Miyaji et al. 2001; Hasinger et al. 2005; Silverman et al. 2008; Croom et al. 2009). However, this statistical approach does not provide sufficient information about the mass of individual SMBHs at various redshifts. A more detailed evolutionary study requires such measurements, in combination with a reliable estimate of the bolometric luminosity ($L_{\rm bol}$) and hence the light-to-mass ratio or, equivalently, the normalized accretion rate $L/L_{\rm Edd} \equiv L_{\rm bol}/L_{\rm Edd}$.

Several recent studies suggest that the more massive BHs experience most of their growth at very early epochs ($z \gtrsim 3$), while those observed as AGNs in the local universe tend to have lower $M_{\rm BH}$ ("downsizing;" e.g., Marconi et al. 2004; Shankar et al. 2009). A similar effect is suggested for the distributions of $L/L_{\rm Edd}$, such that at $z \gtrsim 2$ most AGNs accrete close to their Eddington limit (Merloni 2004; Shankar et al. 2009). It is also predicted that there should be an anticorrelation between $M_{\rm BH}$ and $L/L_{\rm Edd}$ at all redshifts. These trends are in general agreement with observations (e.g., McLure & Dunlop 2004; Netzer & Trakhtenbrot 2007; Shen et al. 2008). Detailed simulations of galaxy mergers predict that the instantaneous AGN luminosity and SMBH accretion rate vary greatly on very short timescales (Di Matteo et al. 2005; Hopkins et al. 2006; Sijacki et al. 2007). The overall BH accretion period following major mergers lasts $\sim$1 Gyr, out of which the central source would appear as a luminous, unobscured AGN for at most a few $\times$ 100 Myr. $M_{\rm BH}$ may grow by as much as a factor $\sim$1000 during such mergers. The merger history of SMBH hosts can also be traced in cosmological simulations of structure formation, by following halo merger trees (e.g., Volonteri et al. 2003). Almost all these models require (or assume) that at $z \gtrsim 3$ most AGNs would accrete close to, or indeed at their Eddington limit. The fast growth has to last almost continuously from very early epochs ($z \sim 20$) and involve massive seed BHs ($M_{\rm seed} \gtrsim 10^3\,M_\odot$) to account for the very massive BHs detected at $z \sim 6$ (e.g., Fan et al. 2006; Volonteri 2010, and references therein). The combination of structure formation models' predictions at $z \sim 3$–6 with the recently observed high clustering of high-redshift luminous AGNs (Shen et al. 2007) suggests that the typical duty cycles—the fraction of the total time involving fast accretion—should remain above 0.5 and probably reach unity (e.g., White et al. 2008; Wyithe & Loeb 2009; Shen et al. 2010; Shankar et al. 2010a; Bonoli et al. 2010). These studies use various prescriptions to link AGNs with their dark matter halos. At lower redshifts (i.e., $z \lesssim 2$), the accretion can be more episodic with a typical duty cycle between $\sim 10^{-3}$ and $\sim$0.1 (e.g., Marconi et al. 2004; Merloni 2004; Shankar et al. 2009). A comprehensive up-to-date review of many of these issues is given in Shankar (2009).

In order to test these scenarios, $M_{\rm BH}$ and $L/L_{\rm Edd}$ ought to be measured in large, representative samples. For unobscured, type-I AGNs, this is usually achieved by using "single epoch" (or "virial") $M_{\rm BH}$ determination methods, which are based on the

* Based on observations collected at the European Organisation for Astronomical Research in the Southern Hemisphere, Chile, as part of programs 081.B-0549, 082.B-0520, and 085.B-0863, and at the Gemini Observatory, as part of programs GN-2007B-Q-56 and GN-2008B-Q-75.

results of long-term reverberation mapping campaigns. These methods are based on estimating the size of the broad-line region (BLR) and involve an empirical relation of the form $R_{\rm BLR} \propto (\lambda L_\lambda)^\alpha$, where λL_λ is the monochromatic luminosity in a certain waveband. Combining $R_{\rm BLR}$ with the assumption of virialized motion of the BLR gas, we get $M_{\rm BH} = f G^{-1} L^\alpha V_{\rm BLR}^2$, where f is a geometrical factor of order unity (e.g., Kaspi et al. 2000; Vestergaard & Peterson 2006; Bentz et al. 2009). The effect of radiation pressure force on such estimates is still a matter of some discussion (Marconi et al. 2008), but recent work suggests that it is not very important (Netzer 2009a; Netzer & Marziani 2010). Single epoch mass estimate methods based on the Hβ and Mg II λ2798 lines (e.g., Kaspi et al. 2005 and McLure & Dunlop 2004, respectively) were used to estimate $M_{\rm BH}$ up to $z \simeq 2$ in large optical surveys (e.g., Corbett et al. 2003; McLure & Dunlop 2004; Netzer & Trakhtenbrot 2007; Fine et al. 2008; Shen et al. 2008). Much smaller samples of $z > 2$ sources were studied by observing Hβ or Mg II in one of the NIR bands (Shemmer et al. 2004, hereafter S04; Kurk et al. 2007, hereafter K07; Netzer et al. 2007, hereafter N07; Marziani et al. 2009; Willott et al. 2010, hereafter W10).

$M_{\rm BH}$ can also be estimated from the broad C IV λ1549 line, using specifically calibrated relations (e.g., Vestergaard & Peterson 2006). This would potentially enable the study of large samples of AGN at high redshifts. However, there is clear evidence that C IV-based estimates of $M_{\rm BH}$ are unreliable. Baskin & Laor (2005) found that the C IV line is often blueshifted with respect to the AGN rest frame, which suggests that the dynamics of the C IVemitting gas may be dominated by nonvirial motion. Several studies of large samples clearly demonstrate that the relation between the widths of the C IV line and of the lower ionization lines (Hβ and Mg II) is weak and shows considerable scatter (e.g., Shen et al. 2008; Fine et al. 2010) that is inconsistent with the virial assumption used in such mass estimators. Finally, our own study (N07) of luminous $z \simeq 2.4$ and $\simeq 3.3$ AGNs shows a complete lack of correlation between C IV-based and Hβ-based estimates of $M_{\rm BH}$. These discrepancies become crucial at high redshifts and large $M_{\rm BH}$ and lead to the conclusion that only Hβ-based and Mg II-based mass estimates are reliable enough to infer the properties of such sources.

Our previous project (S04 and N07) presented the largest sample of $z \simeq 2.4$ and $\simeq 3.3$ type-I AGNs for which $M_{\rm BH}$ and $L/L_{\rm Edd}$ were reliably measured using NIR Hβ spectroscopy. The distribution of $L/L_{\rm Edd}$ at $z \simeq 2.4$ and $\simeq 3.3$ was found to be broad, and about half of the sources had $L/L_{\rm Edd} < 0.2$, inconsistent with several of the models mentioned above. In particular, the typically low accretion rates and the very high masses (up to $\log(M_{\rm BH}/M_\odot) \simeq 10.5$) also mean that $\sim$60% of the sources did not have enough time to grow to the observed $M_{\rm BH}$ by continuous accretion at the observed rates. These findings suggest that an epoch of faster SMBH growth must have occurred, for most objects, at $z > 3.5$. In order to probe such redshifts, the Mg II line must be observed in either the H or the K bands. Practically, this corresponds to focusing on $z \simeq 4.8$ or $z \simeq 6.2$ sources.

In this paper, we present a systematic study of $M_{\rm BH}$ and $L/L_{\rm Edd}$ in a large, well-defined sample of $z \simeq 4.8$ type-I AGNs. This is based on new H-band spectroscopic observations, which enable the measurement of the Mg II line. We describe the sample selection and the observations in Section 2 and the way we deduced $M_{\rm BH}$ and $L/L_{\rm Edd}$ in Section 3. The main results of these measurements are presented in Section 4 and discussed in Section 5 where we compare these results to those of other high-redshift samples. The main findings are summarized in Section 6. Throughout this work, we assume a standard ΛCDM cosmology with $\Omega_\Lambda = 0.7$, $\Omega_M = 0.3$, and $H_0 = 70$ km s^{-1} Mpc^{-1}.

2. SAMPLE SELECTION, OBSERVATIONS, AND DATA REDUCTION

2.1. Sample Selection

Sources were selected to allow the measurement of the Mg II λ2798 emission line and the continuum flux at 3000 Å (F_{3000}), thus providing reliable $M_{\rm BH}$ and $L/L_{\rm Edd}$ estimates. The sources were selected from the sixth data release (DR6; Adelman-McCarthy et al. 2008) of the Sloan Digital Sky Survey (SDSS; York et al. 2000). We first limited our search to quasi-stellar object-class ("QSO"-class) objects with $z \sim 4.65$–4.95, so that the Mg II line and F_{3000} could be observed within the H band. The completeness rate of SDSS spectroscopy for QSOs at this redshift is above 98%, down to a limiting magnitude of $i \simeq 20$ (Richards et al. 2006a). This initial search resulted in 177 objects. Next, we verified that the SDSS-observed C IV lines are of acceptable S/N and that no broad absorption features are present, since these are also expected to appear in the Mg II profile. These criteria reduced the list of candidates to 129 sources.

To estimate the H-band flux of the targets, we extrapolated the rest-frame flux density at 1450 Å to the *observed*-frame flux density at 1.65μm, using the $f_\nu \propto \nu^{-0.44}$ spectral energy distribution (SED) presented by Vanden Berk et al. (2001). We applied a flux limit of $f_\lambda(1450\,\text{Å}) \gtrsim 6 \times 10^{-18}$ erg cm^{-2} s^{-1} Å^{-1}, which translates to $f_\lambda(1.65\,\mu\text{m}) \gtrsim 2.1 \times 10^{-18}$ erg cm^{-2} s^{-1} Å^{-1}, to include only those sources which would provide NIR spectra with S/N $\gtrsim$ 5–10 within reasonable exposure times. This formal flux limit translates to $L_{\rm bol} \simeq 5 \times 10^{46}$ erg s^{-1} (see below). Our flux limit results in the omission of only six candidates, leaving 123 sources. Different observational constraints (a combination of declination, observational seasons etc.; see Section 2.2) forced us to observe only 40 of these 123 candidates. We verified that the distribution of $f_\lambda(1450\,\text{Å})$ for the observed sample is very similar to that of the flux-limited sample of 123 sources, as well as the entire initial sample of 177 SDSS objects. In particular, we find four sources ($\sim$11% of the observed sample) with $f_\lambda(1450\,\text{Å}) \lesssim 7.5 \times 10^{-18}$ erg cm^{-2} s^{-1} Å^{-1} and 15 sources ($\sim$43%) with $f_\lambda(1450\,\text{Å}) \lesssim 1.5 \times 10^{-17}$ erg cm^{-2} s^{-1} Å^{-1}. Given this and the high level of completeness in the SDSS, we consider this sample to be the representative of the complete sample of luminous AGNs at $z \simeq 4.8$.

Several studies suggest that the mass and accretion rate evolution of SMBHs may be connected with their radio properties (see, e.g., McLure & Jarvis 2004; Shankar et al. 2010b, but also Woo & Urry 2002). To determine the radio properties of the $z \simeq 4.8$ sources, we utilized the cross-matched catalog Faint Images of the Radio Sky at Twenty centimeters radio survey (FIRST; Becker et al. 1995; White et al. 1997). Due to the high redshift of our sample, and the relatively low sensitivity of FIRST, most candidates have only upper limits on their radio fluxes, and thus upper limits on the radio loudness ($R_{\rm L} \equiv \frac{f_\nu(5\,\text{GHz})}{f_\nu(4400\,\text{Å})}$; Kellermann et al. 1989). For those sources, we estimated $R_{\rm L}$ based on a 3σ FIRST upper flux limit of $f_\nu(5\,\text{GHz}) = 0.6$ mJy and assuming a radio SED of $f_\nu \propto \nu^{-0.8}$. $f_\nu(4400\,\text{Å})$ was estimated from $f_\lambda(1450\,\text{Å})$ and the Vanden

Table 1
Observation Log

Object ID (SDSS J)	z_{SDSS}[a]	Instrument	Observation Date	Total Exp. Time (s)	*H*-band Magnitude	
					Spectro.[b]	Imaging[c]
000749.17 + 004119.4	4.837	SINFONI	2008 Jun 6 & 29	4200	18.59	(18.1)
003525.28 + 004002.8	4.757	SINFONI	2008 Jun 29 & 30	4200	17.82	(18.0)
021043.15 − 001818.2	4.733	NIRI	2007 Sep 4	6380	18.73	(17.8)
033119.67 − 074143.1	4.738	SINFONI	2008 Oct 1	2400	17.49	
075907.58 + 180054.7	4.861	NIRI	2007 Oct 18 & Nov 11	8100	17.31	
080023.03 + 305100.0	4.687	NIRI	2008 Dec 7	6160	17.06	
080715.12 + 132804.8	4.874	NIRI	2008 Dec 21	4590	17.52	
083920.53 + 352457.6	4.777	NIRI	2008 Dec 15	7290	18.26	
085707.94 + 321032.0	4.776	NIRI	2008 Jan 6	6490	17.06	
092303.53 + 024739.5	4.660	SINFONI	2008 Dec 23 & 2009 Jan 1	6000	18.44	(18.4)
093508.50 + 080114.5	4.699	SINFONI	2008 Dec 20	2400	17.89	17.9
093523.32 + 411518.7	4.836	NIRI	2008 Dec 7 & 12	6440	17.36	
094409.52 + 100656.7	4.748	SINFONI	2010 Mar 23	2400	17.77	
101759.64 + 032740.0	4.917	SINFONI	2008 Nov 28 & 2009 Jan 2	6000	18.63	(18.9)
105919.22 + 023428.8	4.735	SINFONI	2009 Feb 17	2400	17.75	18.0
111358.32 + 025333.6	4.882	SINFONI	2008 Apr 6	3000	17.9	
114448.54 + 055709.8	4.793	SINFONI	2008 Apr 6, 8 & 22	8100	18.56	18.6
115158.25 + 030341.7	4.698	SINFONI	2008 Apr 22	6000	18.94	
120256.44 + 072038.9	4.785	SINFONI	2009 Jan 3 & 6	4800	18.15	18.0
123503.04 − 000331.6	4.723	SINFONI	2008 May 4	8700	18.46	
130619.38 + 023658.9	4.852	SINFONI	2009 Feb 6	3300	16.81	16.9
131737.28 + 110533.1	4.810	SINFONI	2009 Jan 20 & 21	4500	18.01	(17.9)
132110.82 + 003821.7	4.716	SINFONI	2008 Apr 7 & 9	3000	18.4	
132853.67 − 022441.7	4.695	SINFONI	2009 Feb 8	2400	18.07	
133125.57 + 025535.6	4.737	SINFONI	2008 Apr 14 & 26	4800	18.67	18.7
134134.20 + 014157.8	4.670	SINFONI	2009 Feb 8	1800	17.02	
134546.97 − 015940.3	4.714	SINFONI	2008 Apr 26	1800	18.38	
140404.64 + 031404.0	4.870	SINFONI	2010 Mar 28	4500	17.71	17.7
143352.21 + 022714.1	4.721	SINFONI	2010 Mar 29	600	16.7	
143629.94 + 063508.0	4.850	SINFONI	2010 Mar 28	2400	17.79	18.0
144352.95 + 060533.1	4.879	SINFONI	2010 Apr 4	4800	18.56	18.9
144734.10 + 102513.2	4.686	SINFONI	2010 Apr 7 & 8	5400	18.78	(18.6)
151155.98 + 040803.0	4.686	SINFONI	2010 Apr 4	2400	17.99	17.8
161622.11 + 050127.7	4.872	SINFONI	2010 Apr 8	900	16.89	17.3
165436.86 + 222733.7	4.678	NIRI	2007 Aug 19	3480	17.66	
205724.15 − 003018.0	4.663	NIRI	2008 Aug 12	5800	16.77	
220008.66 + 001744.8	4.818	NIRI	2007 Oct 12	6160	17.51	(17.5)
221705.72 − 001307.7	4.689	SINFONI	2008 Apr 19	3300	18.12	(18.4)
222509.16 − 001406.8	4.888	NIRI	2007 Sep 3	6380	17.15	(17.1)
224453.06 + 134631.8	4.657	SINFONI	2010 Jul 6 & 8	4800	18.67	

Notes.
[a] Redshift obtained from the SDSS archive, based on rest-frame UV emission lines.
[b] *H*-band (Vega) magnitude derived from the calibrated spectra by synthetic photometry.
[c] *H*-band (Vega) magnitude derived from direct CTIO/ISPI imaging, or from the UKIDSS database (in parentheses).

Berk et al. (2001) composite. All but five observed targets (see Table 1) have upper limits on R_L which are below ∼40. Two of the remaining sources (J0210-0018 & J1235-0003) have firm FIRST detections (f_ν [5 GHz] = 9.75 and 18.35 mJy, respectively) and are thus considered as radio-loud AGNs ($R_L \simeq 104$ and 1080, respectively). Three additional targets were not observed by FIRST and thus have no viable radio data. In what follows, we verified that the inclusion or exclusion of these five sources does not significantly affect our results. In summary, the 40 $z \simeq 4.8$ AGNs presented here comprise a flux-limited sample which represents a large fraction of all such SDSS sources. In terms of bolometric luminosity, it is complete down to $L_{bol} \simeq 5 \times 10^{46}$ erg s^{-1} and most of the sources are not radio loud. The basic properties of the 40 sources are given in Table 1.

2.2. Spectroscopic Observations and Reduction

The *H*-band spectra of our $z \simeq 4.8$ sample were obtained using the Gemini-North and the Very Large Telescope (VLT) observatories. The campaign was split over several semesters, with brighter targets predominantly observed with the Near Infra-Red Imager instrument (NIRI; Hodapp et al. 2003) on Gemini-North (as part of programs GN-2007B-Q-56 and GN-2008B-Q-75) and fainter ones with the more sensitive SINFONI instrument (Eisenhauer et al. 2003) on the VLT-UT4 (as part of programs 081.B-0549, 082.B-0520, and 085.B-0863). The log of observations is given in Table 1. All the observations were performed in queue/service modes, requested not to exceed an airmass of ∼1.7 and seeing of ∼1″, during clear nights and "gray-time" lunar phase. The 11 Gemini-North/NIRI

targets were observed through a $0\farcs75 \times 110''$ slit and the G5203 grism at the $f/6$ setup, providing $R \sim 520$. The sub-integrations were of ∼300 s, with dithers of $6''$ along the slit after each sub-integration. The 29 VLT/SINFONI targets were observed through the $8'' \times 8''$ field of view (FOV; aka "250 mas spaxel^{-1}") We used SINFONI's "H+K" mode, since the broad Mg II λ2798 line can be resolved well with the resulting $R \sim 1500$. The *K*-band spectra assisted in determining the continuum flux of the SINFONI targets. Sub-integrations were of 150 s or 300 s and (diagonally) dithered by $\sim 6''$ across the FOV. Despite this type of dithering, the spectroscopically resolved OH sky emission contributes a major source of noise to our reduced data (see below). In both observatories, telluric standards of spectroscopic types B, A, and G were observed immediately before or after the science targets, at a similar airmass.

The reduction of the raw data was carried out using the standard pipelines of the respective facilities. We used the GEMINI v.1.8 package in IRAF to co-align and combine the sub-integrated frames while subtracting the sky emission. The one-dimensional spectra were extracted through a typical aperture of 20 pixels which correspond to $\sim 2\farcs3$. The SINFONI v.2.0.5 pipeline (under the ESOREX environment) was used to extract three-dimensional "data cubes" from each sub-integrated frame, which include an individual wavelength calibration. The data cubes were then co-aligned and combined, while the sky emission was estimated from the appropriate dithered pointings. The combined data cube of each source was examined to estimate the actual point-spread function, and an appropriate circular aperture was used to extract the one-dimensional spectra. Due to the varying flexure of the instrument during the long (1 hr) SINFONI observing blocks, there is a noticeable "wavelength flexure" effect in the extracted one-dimensional spectra. This effect results in P-Cygni-like spectral features and can be treated separately (see Davies 2007). We note that the observable properties critical to this work (i.e., L_{3000} and FWHM(Mg II)) are not very sensitive to such narrow ($\lesssim$400 km s^{-1}) OH-originated features.

The spectra of the standard stars were reduced and extracted in the same manner as above, using the same apertures as those used for the science targets. The published spectral types of these stars were used to correct for the instrumental response of each science observations and their published Two Micron All Sky Survey (2MASS; Cutri et al. 2003) magnitudes were used to flux-calibrate the science spectra. The typical photometric error associated with the 2MASS magnitudes is $\lesssim$10%.

2.3. Photometric Observations

Wide-field *H*- and *K*-band imaging for 11 of the $z \simeq 4.8$ sources was obtained at the CTIO Blanco telescope, with the ISPI instrument (van der Bliek et al. 2004). We aimed at having at least three bright 2MASS stars observed in the same field for each of the science targets. Each field was imaged to achieve S/N $\gtrsim$ 20 for the science targets, through a series of dithered short exposures, to avoid saturation. The CTIO observations were carried out with mostly clear conditions, with seeing of $\sim 1''$, during a single run on the night of 2010 March 4. The raw imaging data were reduced following standard procedures, including bad pixel removal, dark and flat calibration, and co-alignment of the sub-exposures. Aperture photometry was performed over the science targets and the several visible 2MASS stars in each field. Whenever possible, we used only stars with best-quality 2MASS photometry for the relative scaling of the science target fluxes. The magnitudes thus obtained are listed in Table 1, for the relevant sources.

Since the spectroscopy and imaging observations were not simultaneous, there exists a real uncertainty regarding possible flux variability of our $z \simeq 4.8$ sources. Our targets are relatively luminous, and thus are not expected to have large variability amplitudes (e.g., Bauer et al. 2009 and references therein). We compared the photometric and the spectroscopic fluxes, achieved by synthetic photometry of the SINFONI and NIRI spectra. The median discrepancy is $\lesssim$ 0.09 mag, in the sense that the (later observed) photometric fluxes are on average fainter than the spectroscopy-deduced fluxes. The standard deviation is close to 0.2 mag. Photometric fluxes for 10 additional sources were obtained through the fourth data release of the UKIRT Infrared Digital Sky Survey (UKIDSS/DR4; Lawrence et al. 2007). The photometry of these sources is also consistent with the fluxes deduced from our spectrophotometric calibration. Excluding one significant outlier (J0210−0018), the standard deviation between the two methods is, again, close to 0.2 mag.

With this evidence of little flux variation, and reliable spectrophotometry for a large fraction (∼50%) of arbitrary selected sources, we conclude that the accuracy of our spectrophotometric flux calibration is high, with uncertainties of about 10%–15%. In order to correctly probe the instantaneous emission from the sources, we thus adopt the spectrophotometric fluxes to measure luminosities, even for those sources which were photometrically observed. The full set of calibrated spectra is presented in Figure 1.

3. LINE FITTING, AND $M_{\rm BH}$ AND $L/L_{\rm Edd}$ DETERMINATION

3.1. Line Fitting

To determine $M_{\rm BH}$ and $L/L_{\rm Edd}$, we fit the observed spectra with a model that combines a continuum component, Fe II and Fe III lines, and the two doublet Mg II lines. The procedure used here is similar to the one presented in several other studies (e.g., Shen et al. 2008 and references therein). It is based on a new code that was developed and extensively tested on a large sample of $0.5 \lesssim z \lesssim 2$ SDSS type-I AGNs, and will be described in detail in a future publication (B. Trakhtenbrot et al. 2011, in preparation). In particular, this large sample was used to verify that important quantities such as narrow emission lines and bolometric corrections are consistent with those derived from the well-studied Hβ-[O III] λ5007 emission region (rest-frame wavelengths of 4600–5100 Å). This was done using a subsample of ∼5000 sources at $0.5 \lesssim z \lesssim 0.75$, where the SDSS spectra show both the Hβ and Mg II lines.

The fitting of the $z \simeq 4.8$ AGNs was preformed individually, verifying a satisfactory match between the data and the model. As a first step, a linear pseudocontinuum is fit to the flux around 2655 and 3020 Å. Next, we fit the Fe II and Fe III emission complexes redward and blueward of Mg II. For this we use a template made of the composite prepared by Vestergaard & Wilkes (2001) that was supplemented by several predicted Fe II lines (kindly provided by G. Ferland). These are mainly Fe II emission lines which coincide in wavelength with the Mg II line, where the observationally based template of Vestergaard & Wilkes (2001) is incomplete. This part of the template is very similar to the models presented in Sigut & Pradhan (2003, their Figure 13) and in Baldwin et al. (2004, their Figure 5). In both cases, the Fe II flux under the Mg II line is dominated by the red

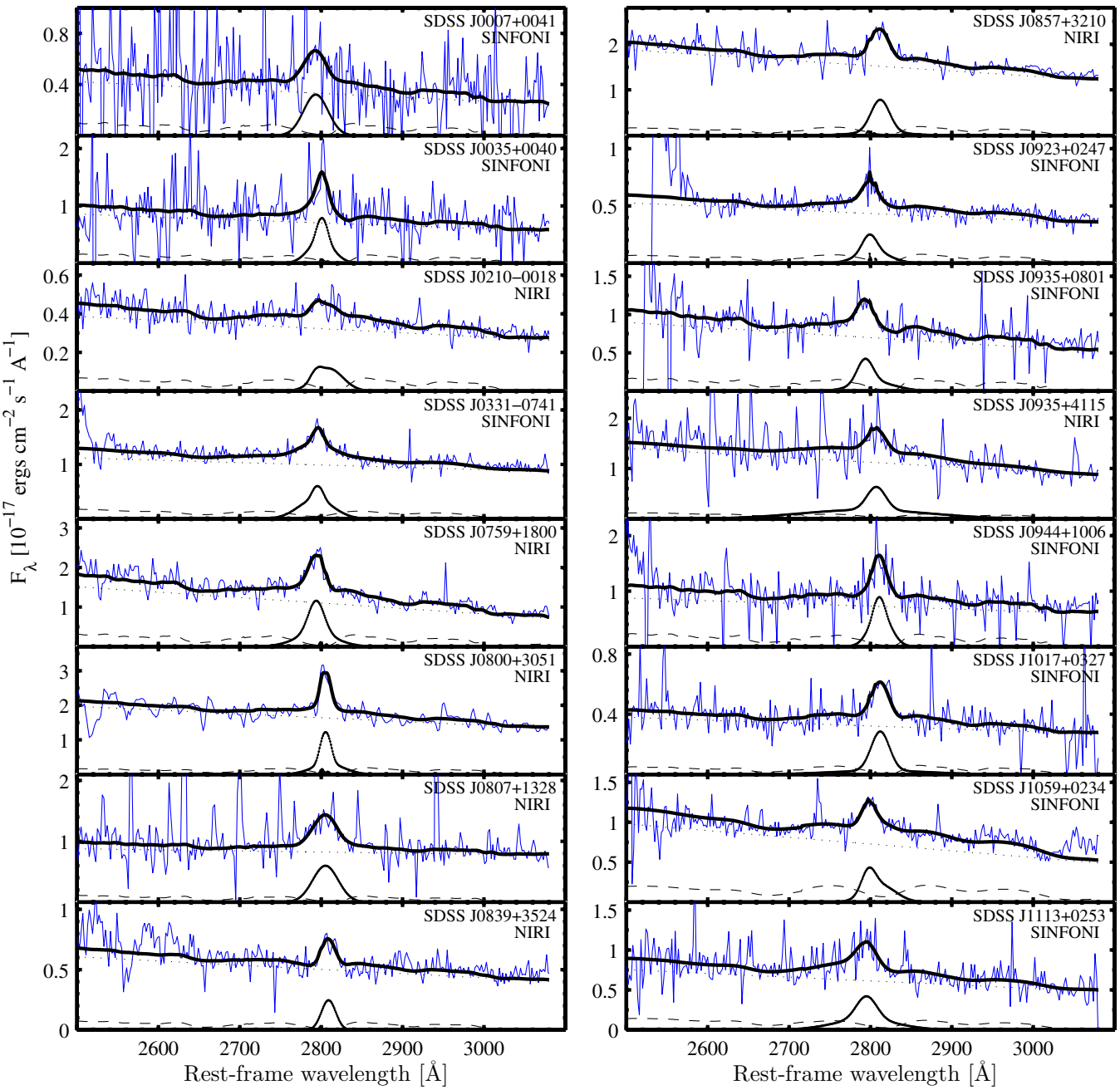

Figure 1. Rest-frame spectra of the $z \simeq 4.8$ sources under study. The spectra are ordered by increasing right ascension. In each panel, we show the observed flux density (thin blue line) and the best-fit model (thick black line), which is composed of a continuum component (dotted line), an Fe II & Fe III emission complex (thin dashed curve), and the total (two-component) Mg II λ2798 line (thin black lines).

(A color version of this figure is available in the online journal.)

extension of the ∼2750 Å emission complex. The additional Fe II flux tends to flatten in sources with very broad lines, but the overall effect on the Mg II line fitting is very small. We consider this template to be more reliable than the addition of constant flux under the Mg II line, adopted by Kurk et al. (2007) and Fine et al. (2008). Several other studies, such as Salviander et al. (2007) and Shen et al. (2008), use templates very similar to ours, following the models in Sigut & Pradhan (2003).

Our basic iron template is based on a single line profile with FWHM $\simeq$ 1175 km s^{-1}. To account for the range of observed line widths, we created a grid of broadened Fe templates, by convolving the basic template with single Gaussian profiles of varying width, ranging from FWHM = 1200 to 10,000 km s^{-1}. We note that the templates that correspond to FWHM $\gtrsim$ 4000 km s^{-1} lack almost any distinguishable emission features. The grid of broadened Fe templates is fitted to the continuum-subtracted spectra over the rest-frame wavelength regions of 2600–2700 Å and 2900–3030 Å, and the best-fit template is chosen by standard χ^2 minimization. We allow the Fe template to be shifted with respect to the systemic redshift and for its width to differ from that of the Mg II line. After the subtraction of the best-fit Fe template, the pseudocontinuum is re-fitted and we iterate the Fe-fitting process once again. This is done to ensure the convergence of the best-fit pseudocontinuum and Fe lines. The final measure of the pseudocontinuum flux, f_λ(3000 Å), provides the continuum luminosity L_{3000} which is further used

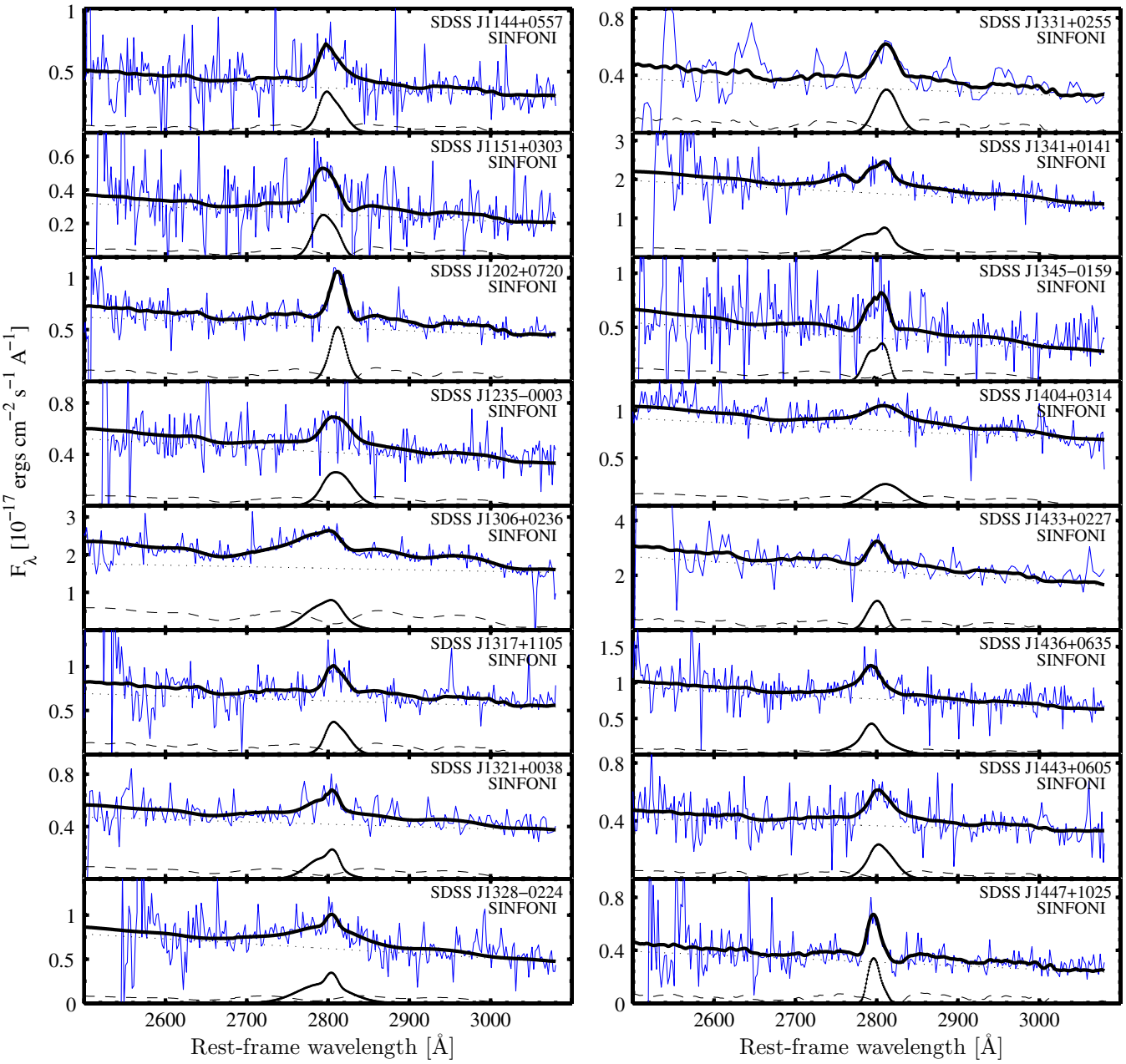

Figure 1. (Continued)

to calculate $M_{\rm BH}$ and $L/L_{\rm Edd}$. It is important to note that the L_{3000} thus obtained is *not* the intrinsic, underlying AGN continuum as it also includes a contribution from the Balmer continuum emission, that is not accounted for by the fitting procedure.

Once the pseudocontinuum and Fe contributions are subtracted, we fit the Mg II line itself. The model for the line consists of three Gaussians, two broad and one narrow component for each of the Mg II doublet lines. The intensity ratio of the doublet components is fixed to 1:1, suitable for optically thick lines. The broad components are limited to line widths in the range $1200\,{\rm km\,s^{-1}} < {\rm FWHM} < 10{,}000\,{\rm km\,s^{-1}}$, while the width of the narrow components is bound to $300\,{\rm km\,s^{-1}} < {\rm FWHM} < 1200\,{\rm km\,s^{-1}}$. Although the relative contribution of the narrow components is very small (<10%), the procedure reproduces well the narrow-line region (NLR) width. This was verified by comparing the NLR–FWHM resulting from the (separate) Mg II and Hβ fitting for the test sample of ∼5000 sources at $0.5 \lesssim z \lesssim 0.75$ mentioned above. We have also included a single absorption feature (also a Gaussian) to account for the appearance of blueshifted Mg II troughs. The best-fit model is used to measure the FWHM of the total broad *single* Mg II line and the total luminosity of both Mg II components. We stress that in earlier studies, the line width was calculated using the combined doublet profile, which has implications to the deduced $M_{\rm BH}$ (see Section 5.1). The best-fit continuum and Mg II line parameters are given in Table 2. The uncertainties that also appear in Table 2 reflect the true uncertainties associated with the spectroscopic reduction and line-fitting procedure. These were estimated from varying several of the parameters involved in these processes[4] and examining the range of possible outcomes.

[4] For example, varying flux calibrations for sources which were observed during several nights, the shape and normalization of the Fe II template and the possible identification of absorption features.

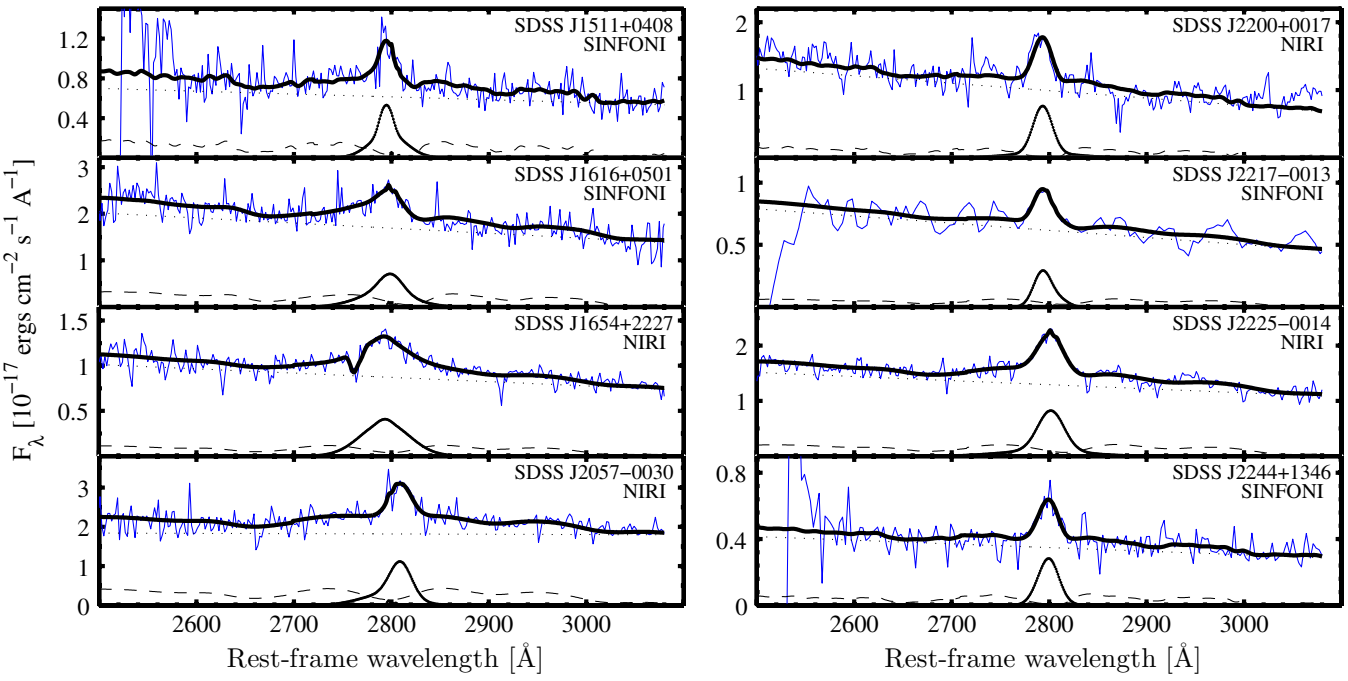

Figure 1. (Continued)

We consider these uncertainties to be much more realistic than those derived solely from the flux noise.

3.2. Estimating $M_{\rm BH}$ and $L/L_{\rm Edd}$

The $L_{\rm bol}$ and $M_{\rm BH}$ estimates used in this work are based on the measured L_{3000} and FWHM(Mg II). For the latter, we adopt the McLure & Dunlop (2004) relationship:

$$M_{\rm BH} = 3.2 \times 10^6 \left[\frac{L_{3000}}{10^{44}\,{\rm erg\,s^{-1}}}\right]^{0.62} \left[\frac{\rm FWHM(Mg\,II)}{10^3\,{\rm km\,s^{-1}}}\right]^2 M_\odot\,. \quad (1)$$

To estimate $L_{\rm bol}$, we have to assign a bolometric correction factor, $f_{\rm bol}(\lambda) = L_{\rm bol}/\lambda L_\lambda$. For this we adopt the Marconi et al. (2004) luminosity-dependent SED, which also provides a polynomial prescription for estimating $f_{\rm bol}(4400\,\text{Å})$. The prescription can be used with other UV–optical monochromatic luminosities, by adopting the Vanden Berk et al. (2001) UV continuum ($f_\nu \propto \nu^{-0.44}$). Our procedure relies on our own empirically calibrated $f_{\rm bol}(3000\,\text{Å})$ versus L_{3000} relation, derived using the $0.5 \lesssim z \lesssim 0.75$ type-I SDSS AGN test sample. For each source, we measured both L_{5100} and L_{3000} and converted L_{5100} to $L_{\rm bol}$ using the relation of Marconi et al. (2004) and the Vanden Berk et al. (2001) template. This provides, for each of the ∼5000 sources, both L_{3000} and $f_{\rm bol}(3000\,\text{Å}) = L_{\rm bol}/L_{3000}$. The best-fit relation is

$$f_{\rm bol}(3000\,\text{Å}) = -0.58\mathcal{L}^3_{3000,44} + 3.85\mathcal{L}^2_{3000,44} - 8.38\mathcal{L}_{3000,44} + 9.34, \quad (2)$$

where $\mathcal{L}_{3000,44} \equiv \log(L_{3000}/10^{44}\,{\rm erg\,s^{-1}})$. The bolometric corrections for our $z \simeq 4.8$ sample range between 3.35 for the least luminous source and 3.43 for the most luminous one. The typical $f_{\rm bol}(3000\,\text{Å})$ is lower than those used in other studies (e.g., Elvis et al. 1994; Richards et al. 2006b) by a factor of about 1.5. This is mostly due to the fact that the Marconi et al. (2004) estimates of $L_{\rm bol}$ do not include most of the mid- to far-IR emission, which originates from dust around the central source. The normalized accretion rate is $L/L_{\rm Edd} = L_{\rm bol}/(1.5 \times 10^{38}\,M_{\rm BH}\,M_\odot^{-1})$ that is appropriate for ionized gas with solar metallicity. The deduced $M_{\rm BH}$ and $L/L_{\rm Edd}$ are given in Table 2.

We have also estimated $M_{\rm BH}$ from the C IV λ1549 line, that is observed in the SDSS spectrum of each source. The line-fitting procedure was similar to the one described above for Mg II and also to those discussed in other studies (e.g., Shen et al. 2008; Fine et al. 2010). We calculated $M_{\rm BH}$ from L_{1450} and FWHM(C IV) following the prescription of Vestergaard & Peterson (2006). We find that the C IV line is systematically broader than Mg II, similar to the recent finding of Fine et al. (2010). The differences in widths translate to higher C IV-based $M_{\rm BH}$ estimates, with respect to those derived from Mg II. These findings confirm the suspicion about the problematic use of the C IV-based method (see Section 1). A full analysis of these issues is deferred to a future publication. In what follows, we rely solely on the Mg II-based measurements of $M_{\rm BH}$ and $L/L_{\rm Edd}$.

4. RESULTS

4.1. $M_{\rm BH}$ and $L/L_{\rm Edd}$ Distributions

The distributions of $M_{\rm BH}$ and $L/L_{\rm Edd}$ for the $z \simeq 4.8$ sample are shown in Figure 2. They cover the range $8.03 < \log(M_{\rm BH}/M_\odot) < 9.82$ and $0.18 < L/L_{\rm Edd} < 3.92$. The median values and 68% percentiles (taken to be symmetric around the medians) correspond to $\langle \log(M_{\rm BH}/M_\odot)\rangle = 8.89^{+0.32}_{-0.34}$ and $\langle L/L_{\rm Edd}\rangle = 0.59^{+0.63}_{-0.30}$.

As explained in Section 3, both $M_{\rm BH}$ and $L/L_{\rm Edd}$ are derived directly from L_{3000}, and both distributions are affected by the flux limit of the sample. The 1450 Å flux limit corresponds to $f_\lambda(3000\,\text{Å}) \gtrsim 2.1 \times 10^{-18}\,{\rm erg\,cm^{-2}\,s^{-1}\,Å^{-1}}$ which, at $z \simeq 4.8$, gives a limiting luminosity of $L_{3000} \simeq 10^{46}\,{\rm erg\,s^{-1}}$. The limiting $M_{\rm BH}$ is estimated by combining the limiting L_{3000} and FWHM $= 1500\,{\rm km\,s^{-1}}$ using Equation (1). This line width is the minimal width of *any* emission line for which the SDSS pipeline labels the target as a spectroscopic target of type "QSO;" a pre-requirement of our sample selection. We thus

Table 2
Observed and Derived Properties

Object ID (SDSS J)	$z_{\rm SDSS}$	$z_{\rm Mg\,II}$[a]	log L_{1450}[b] (erg s^{-1})	log L_{3000} (erg s^{-1})	L-qual.[c]	log $L_{\rm bol}$ (erg s^{-1})	FWHM(Mg II) (km s^{-1})	FWHM-qual.[d]	log $M_{\rm BH}$ ($M_\odot$)	log $L/L_{\rm Edd}$
000749.17+004119.4	4.837	4.786	46.39	46.04	3	46.57	3665	3	8.90	−0.51
003525.28+004002.8	4.757	4.759	46.35	46.38	3	46.91	1805	3	8.49	0.24
021043.15-001818.2	4.733	4.713	46.66	46.04	2	46.56	4583	3	9.09	−0.70
033119.67-074143.1	4.738	4.729	46.76	46.55	1	47.09	2360	1	8.83	0.08
075907.58+180054.7	4.861	4.804	46.46	46.54	1	47.07	2717	1	8.95	−0.05
080023.03+305100.0	4.687	4.677	46.82	46.73	1	47.26	1404	1	8.49	0.59
080715.12+132804.8	4.874	4.885	46.71	46.53	2	47.07	3837	3	9.24	−0.35
083920.53+352457.6	4.777	4.795	46.70	46.24	2	46.77	1971	2	8.49	0.11
085707.94+321032.0	4.776	4.801	46.94	46.72	2	47.25	2851	2	9.10	−0.03
092303.53+024739.5	4.660	4.659	46.33	46.14	1	46.67	2636	1	8.68	−0.18
093508.50+080114.5	4.699	4.671	46.62	46.33	2	46.87	2714	2	8.82	−0.13
093523.32+411518.7	4.836	4.802	46.66	46.58	2	47.12	3447	3	9.18	−0.24
094409.52+100656.7	4.748	4.771	46.64	46.40	2	46.93	2128	2	8.65	0.11
101759.64+032740.0	4.917	4.943	46.27	46.10	1	46.63	2822	1	8.71	−0.26
105919.22+023428.8	4.735	4.789	46.65	46.36	2	46.89	2899	2	8.89	−0.18
111358.32+025333.6	4.882	4.870	46.49	46.35	2	46.89	3793	3	9.12	−0.41
114448.54+055709.8	4.793	4.790	46.13	46.11	3	46.63	3215	2	8.83	−0.37
115158.25+030341.7	4.698	4.687	46.05	45.91	3	46.44	3741	3	8.84	−0.57
120256.44+072038.9	4.785	4.810	46.28	46.27	1	46.80	2171	1	8.59	0.04
123503.04-000331.6	4.723	4.700	46.07	46.12	2	46.65	4422	3	9.11	−0.64
130619.38+023658.9	4.852	4.860	46.57	46.82	1	47.35	5340	1	9.71	−0.54
131737.28+110533.1	4.810	4.744	46.39	46.34	2	46.87	3144	2	8.95	−0.25
132110.82+003821.7	4.716	4.726	46.47	46.17	2	46.70	3651	3	8.98	−0.45
132853.67-022441.7	4.695	4.658	46.42	46.28	2	46.81	3815	2	9.08	−0.45
133125.57+025535.6	4.737	4.762	46.15	46.02	3	46.55	3445	3	8.83	−0.46
134134.20+014157.8	4.670	4.689	46.87	46.73	2	47.26	6480	2	9.82	−0.74
134546.97-015940.3	4.714	4.728	46.62	46.08	2	46.60	3412	2	8.86	−0.43
140404.64+031404.0	4.870	4.903	46.55	46.49	2	47.02	5360	2	9.51	−0.66
143352.21+022714.1	4.721	4.722	47.14	46.84	2	47.37	2622	2	9.11	0.09
143629.94+063508.0	4.850	4.817	46.62	46.44	2	46.98	3052	2	8.99	−0.19
144352.95+060533.1	4.879	4.884	46.44	46.16	3	46.69	3609	3	8.96	−0.45
144734.10+102513.2	4.686	4.679	46.29	45.99	1	46.51	1407	1	8.03	0.30
151155.98+040803.0	4.686	4.670	46.62	46.32	2	46.86	1735	2	8.42	0.26
161622.11+050127.7	4.872	4.869	47.08	46.80	2	47.33	3910	1	9.43	−0.27
165436.86+222733.7	4.678	4.717	47.14	46.48	1	47.02	5637	1	9.55	−0.70
205724.15-003018.0	4.663	4.680	47.04	46.83	2	47.36	3050	2	9.23	−0.05
220008.66+001744.8	4.818	4.804	46.70	46.51	2	47.04	2404	2	8.82	0.04
221705.72-001307.7	4.689	4.676	46.44	46.28	3	46.81	2274	3	8.63	0.00
222509.16-001406.8	4.888	4.890	46.97	46.70	1	47.23	3504	1	9.27	−0.21
224453.06+134631.8	4.657	4.656	46.30	46.06	2	46.58	2516	2	8.58	−0.17

Notes.
[a] Redshift measured from the best-fit models of the Mg II lines.
[b] Monochromatic luminosity at rest wavelength 1450 Å, obtained from the SDSS/DR6 spectra and redshifts.
[c] Quality flag associated with L_{3000}. Quality flags of "1," "2," and "3" correspond to calibration and/or continuum measurement uncertainties of ∼10%, ∼20%, and ∼40%, respectively.
[d] Quality flag associated with FWHM(Mg II). Quality flags of "1," "2," and "3" correspond to uncertainties of ∼10%, 20%–30% and ∼50%, respectively.

obtain $\log(M_{\rm BH}/M_\odot)_{\rm limit} \simeq 8$. Indeed, one of our sources (J1447+1025) has very similar properties, in terms of L_{3000}, FWHM(Mg II) and $M_{\rm BH}$. However, this source looks as an outlier in the $M_{\rm BH}$ distribution. The next smallest source has $\log(M_{\rm BH}/M_\odot) \simeq 8.4$, which represents the low end of the $M_{\rm BH}$ distribution much better. We conclude that our sample is complete down to $\log(M_{\rm BH}/M_\odot) \simeq 8$, and the fact that we observe (almost) no sources with $\log(M_{\rm BH}/M_\odot) < 8.5$ is a real characteristic of the population of spectroscopically observed, optically selected type-I AGNs at $z \simeq 4.8$.

The limiting $L/L_{\rm Edd}$ is deduced by combining the lowest L_{3000} with FWHM(MgII) = 10,000 km s^{-1}, the upper boundary that FWHM(Mg II) can take in our line-fitting procedure (see Section 3.1). The resulting limiting value is $(L/L_{\rm Edd})_{\rm limit} \simeq 0.04$. Clearly, the limiting $L/L_{\rm Edd}$ is a factor of ∼4.5 below the lowest $L/L_{\rm Edd}$ we actually observe. This reflects the fact that the broadest Mg II line we observe has FWHM(MgII) $\simeq$ 6,500 km s^{-1}.

The highest observable $L/L_{\rm Edd}$ is determined by a combination of the narrowest observable FWHM(Mg II) and the highest luminosities. For instance, the faint and narrow-lined source J1447+1025 is one of the higher $L/L_{\rm Edd}$ sources in our sample. On the other hand, the *highest* $L/L_{\rm Edd}$ source (J0800+3051) has a similarly narrow Mg II line but is among the most luminous sources in the sample (a factor of ∼5.6 more luminous than J1447+1025), thus approaching $L/L_{\rm Edd} \simeq 4$. Since there are

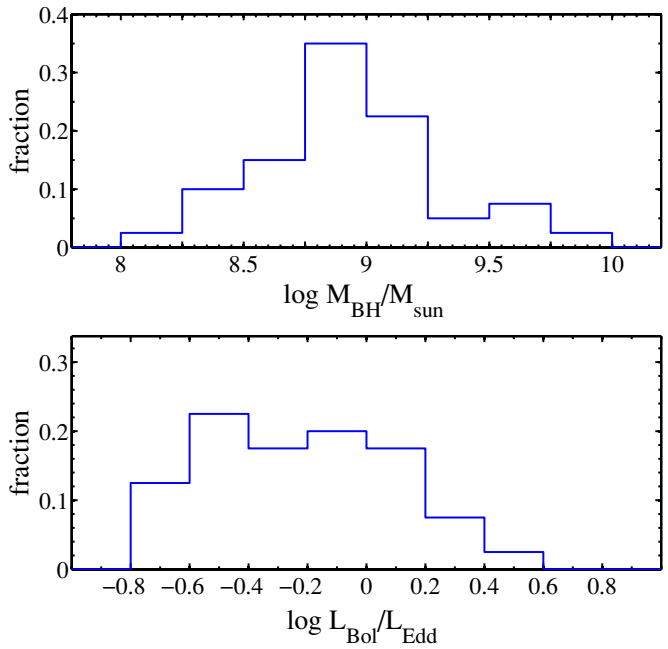

Figure 2. Distributions of $M_{\rm BH}$ (top) and $L/L_{\rm Edd}$ (bottom) for the $z \simeq 4.8$ sample.
(A color version of this figure is available in the online journal.)

no brighter $z \simeq 4.8$ sources in the entire SDSS/DR6 database, we conclude that our sample unveils the highest $L/L_{\rm Edd}$ ($\simeq$4) sources at $z \simeq 4.8$. We also note that $\sim$1/4 of the AGNs in our sample have $1 < L/L_{\rm Edd} \lesssim 4$. Several studies (e.g., Mineshige et al. 2000; Wang & Netzer 2003; Kurosawa & Proga 2009) have shown that such high $L/L_{\rm Edd}$ can be produced in several types of accretion disks.

4.2. The Growth Times of SMBHs from $z = 20$ to $z \simeq 4.8$

Given the observed $M_{\rm BH}$, $L_{\rm bol}$, and $L/L_{\rm Edd}$, we can constrain the lifetimes of the SMBHs in our sample. We first assume that accretion proceeds with a constant $L/L_{\rm Edd}$. This results in an exponential growth of $M_{\rm BH}$, with an e-folding time (Salpeter time) of

$$\tau = 4 \times 10^8 \frac{\eta/(1-\eta)}{L/L_{\rm Edd}} \ {\rm yr}, \quad (3)$$

where η is the radiative efficiency ($L_{\rm bol} = \eta \dot{M}_{\rm infall} c^2$). The time required to grow by such accretion from a seed BH of mass $M_{\rm seed}$ to $M_{\rm BH}$ is

$$t_{\rm grow} = \tau \ \ln\left(\frac{M_{\rm BH}}{M_{\rm seed}}\right) \ {\rm yr}. \quad (4)$$

Despite several attempts to estimate η (e.g., Volonteri et al. 2005; King et al. 2008; and references therein), its typical value and redshift dependence are poorly constrained. A broad range of $\eta \simeq 0.05$–0.3 is required to match the local BH mass function to the integrated accretion history of SMBHs (e.g., Shankar et al. 2004; Wang et al. 2009; Shankar et al. 2010a). There is an even broader range of possible values of $M_{\rm seed}$, depending on the various mechanisms to produce such objects. Remnants of population-III stars would result in $M_{\rm seed} \sim 10$–$100\,M_\odot$ (e.g., Heger & Woosley 2002), while collapse models of either dense stellar clusters or gas halos predict seed masses as large as $M_{\rm seed} \sim 10^3$–$10^6\,M_\odot$ (e.g., Begelman et al. 2006; Devecchi & Volonteri 2009; see Volonteri 2010 for a review). For the sake of consistency with earlier $z > 2$ studies (N07), we assume here $\eta = 0.1$ and $M_{\rm seed} = 10^4\,M_\odot$. With this choice of η, the e-folding times in our sample range from $\sim$10 to $\sim$240 Myr and the faster accreting 50% of the sources show $\tau \lesssim 75$ Myr. Such SMBHs can increase their mass by a factor of $\sim$750 within $\sim$500 Myr. We compared the growth of the SMBHs in our sample up to $z \simeq 4.8$ with the corresponding age of the universe at that redshift ($t_{\rm Universe} \simeq 1.21$ Gyr). The assumption of continuous, constant $L/L_{\rm Edd}$ growth for such a long period is, of course, somewhat simplistic, given the timescales of standard accretion disks (a review of this and related issues can be found in King 2008). About 65% of the sources have $t_{\rm growth} < t_{\rm universe}$. This is a larger fraction than observed in lower redshift samples, which suggests that $z \simeq 4.8$ might represent the sought after episode of fast growth for most SMBHs.

We also calculated the regress of $M_{\rm BH}$ with increasing redshift assuming the aforementioned exponential growth scenario, up to $z = 20$. These evolutionary tracks are shown in Figure 3. The point at which such tracks cross the y-axis in Figure 3 can be regarded as the value of $M_{\rm seed}$ required to match the observed $M_{\rm BH}$ at $z \simeq 4.8$, given the assumption of a constant $L/L_{\rm Edd}$ growth. The diagram demonstrates how the $z \simeq 4.8$ sample can constrain the different BH formation and growth scenarios. For example, about 40% of the $z \simeq 4.8$ sources could have grown from seed BHs with $M_{\rm seed} < 100\,M_\odot$, i.e., stellar-remnant BHs. A further $\sim$20% could have grown from BH seeds with $1000\,M_\odot < M_{\rm seed} < 10^5\,M_\odot$, and another $\sim$20% from BH seeds with $10^5\,M_\odot < M_{\rm seed} < 10^7\,M_\odot$. The remaining lowest $L/L_{\rm Edd}$ sources ($\sim$10%) have $10^7\,M_\odot < M_{\rm seed} < 10^8\,M_\odot$.[5] Since even the most extreme scenarios cannot produce such high $M_{\rm seed}$ (Volonteri 2010), these sources had to accrete at higher rates in the past in order to attain their measured mass. Another explanation is a combination of massive seed BHs with low spins (i.e., small η) at very early epochs. For example, if we assume $\eta = 0.05$, then at $z = 20$ *all* the sources have an implied $M_{\rm seed} < 10^6\,M_\odot$. As mentioned above, the radiative efficiency could be higher, e.g., $\sim$0.2–0.3. Assuming such high values of η in our calculations naturally leads to the requirement of more massive seed BHs. For example, in the extreme case of $\eta = 0.3$ in all sources, we find that 95% of the seed BHs would have $M_{\rm seed} > 500\,M_\odot$.

5. DISCUSSION

5.1. Comparison with Other Studies

Our main goal is to identify the epoch at which most SMBHs experienced the first episode of fast growth. We focus on a comparison of our $z \simeq 4.8$ sample to several $z > 2$ samples with reliably measured $M_{\rm BH}$ and $L/L_{\rm Edd}$. In S04 and N07, we studied a sample of 44 $z \simeq 2.4$ and $\simeq$3.3 type-I AGNs using NIR spectroscopy to measure L_{5100} and FWHM(Hβ). The study showed that a large fraction of the high $M_{\rm BH}$ sources accrete at a rate that is well below the Eddington limit. Assuming these sources accrete at constant $L/L_{\rm Edd}$, such accretion rates cannot explain their measured masses and are in contradiction with several theoretical predictions. Having obtained new data on the $z \simeq 4.8$ sample, we can now compare several groups of AGNs, at several epochs, in an attempt to follow their growth all the way from $z \simeq 6.2$ to $z \simeq 2.4$.

[5] Alternatively, assuming $M_{\rm seed} = 10^4\,M_\odot$, these SMBHs have growth times that are about twice the age of the universe at the corresponding redshift.

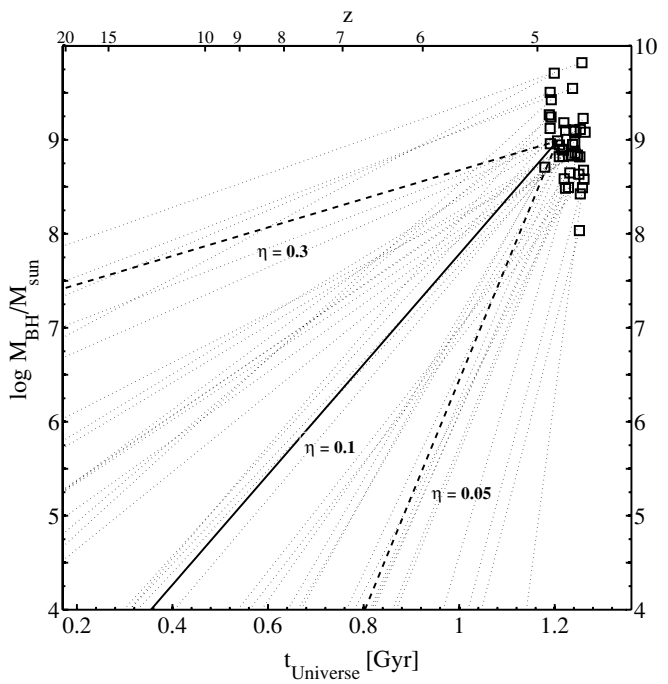

Figure 3. Calculated growth of $M_{\rm BH}$ from $z = 20$ to $z \simeq 4.8$. Black squares represent the masses of the $z \simeq 4.8$ sources and the dotted lines show the regress in $M_{\rm BH}$, assuming exponential growth with the observed $L/L_{\rm Edd}$ and $\eta = 0.1$. The thick lines illustrate a choice of different values of η for a particular source (J1436+0635) which has $M_{\rm BH}$ and $L/L_{\rm Edd}$ that resemble the sample's median values.

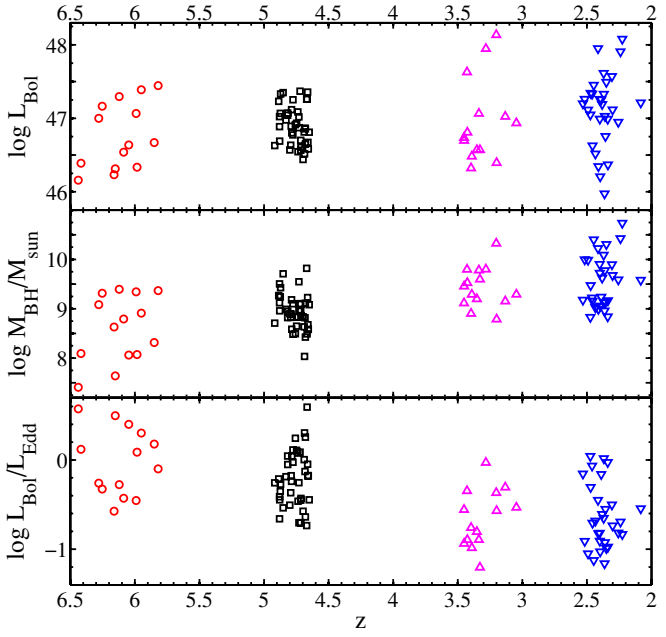

Figure 4. $L_{\rm bol}$, $M_{\rm BH}$, and $L/L_{\rm Edd}$ vs. redshift, for samples of different redshifts discussed in the text: the new $z \simeq 4.8$ sample presented here (black squares), the $z \simeq 2.4$ and $\simeq 3.3$ samples of S04 and N07 (magenta and blue triangles) and the combined $z \simeq 6.2$ sample from K07 and W10 (red circles).

(A color version of this figure is available in the online journal.)

The samples we consider here are the new one at $z \simeq 4.8$ and our earlier (S04 and N07) samples at $z \simeq 2.4$ and $\simeq 3.3$. We also consider a small number of sources at $z \simeq 6.2$ from the samples studied by K07 and W10, which have five and nine reliable $M_{\rm BH}$ and $L/L_{\rm Edd}$ measurements, respectively. These small samples do *not* have a common flux limit and simply represent the up-to-date collection of the sources discovered at those redshifts that were also observed in follow-up NIR spectroscopy. As such, they are not representative of the AGN population at $z \simeq 6.2$. This, along with the small size of the samples, limits their statistical usefulness. To use the data from the $z \simeq 6.2$ samples, we re-calculated $M_{\rm BH}$ and $L_{\rm bol}$ using the methods described above. First, we corrected the published FWHM(Mg II) according to the assumption of only one of the doublet components. This reduces FWHM(Mg II) by a mean factor of $\sim$1.2 and the reported $M_{\rm BH}$ by a mean factor of $\sim$1.44. Second, the smaller $f_{\rm bol}\left(3000\,\text{Å}\right)$ adopted here reduces the reported $L_{\rm bol}$ by a factor of $\sim$1.49. Regarding $L/L_{\rm Edd}$, the two corrections almost completely cancel out.

In Figure 4, we present $L_{\rm bol}$, $M_{\rm BH}$, and $L/L_{\rm Edd}$ for the new $z \simeq 4.8$ sample, the $z \simeq 2.4$ and $\simeq 3.3$ samples of S04 and N07, and the combined sample of $z \simeq 6.2$ AGNs. The four samples suggest an increasing $M_{\rm BH}$ and decreasing $L/L_{\rm Edd}$ with cosmic time. This is better illustrated in Figure 5, where we present the cumulative distribution functions (CDFs) of $M_{\rm BH}$ and $L/L_{\rm Edd}$. The increase in the median $M_{\rm BH}$ and the decrease in the median $L/L_{\rm Edd}$ as a function of decreasing redshift are evident. In particular, there is a clear shift of $\sim$0.5 dex between the median $M_{\rm BH}$ values of the $z \simeq 4.8$ and $z \simeq 3.3$ samples, in the sense of a lower $M_{\rm BH}$ at $z \simeq 4.8$. There is also an opposite shift between the median $L/L_{\rm Edd}$ values. The differences between the $z \simeq 3.3$ and the $z \simeq 2.4$ samples are much smaller, although the $z \simeq 2.4$ sample includes several sources with extremely massive BHs ($\log(M_{\rm BH}/M_\odot) > 10$) which are not observed at earlier epochs. Regarding $M_{\rm BH}$, only $\sim$14% of the $z \simeq 3.3$ sample (two sources) lie below the median value of the $z \simeq 4.8$ sample ($\log(M_{\rm BH}/M_\odot) = 8.92$). Similarly, only $\sim$13% of the $z \simeq 4.8$ sample (five sources) lie above the median value of the $z \simeq 3.3$ sample ($\log(M_{\rm BH}/M_\odot) = 9.37$) and even less ($\sim$6%; two sources) lie above the median value of the $z \simeq 2.4$ sample ($\log(M_{\rm BH}/M_\odot) = 9.59$).

We have further tested the significance of these differences by performing a series of two sample Kolmogorov–Smirnov tests. The null hypothesis that the observed distributions of $L/L_{\rm Edd}$ at $z \simeq 4.8$ and at $z \simeq 3.3$ (or at $z \simeq 2.4$) are drawn from the same parent distribution is rejected with significance levels >99%. A similar test was applied to the $z \simeq 4.8$ and $z \simeq 6.2$ samples, and could not reject the null hypothesis, suggesting that the distributions of $L/L_{\rm Edd}$ at $z \simeq 4.8$ and $z \simeq 6.2$ are statistically similar. We obtain similar results when comparing the distribution of $M_{\rm BH}$ at $z \simeq 4.8$ to that of the $z \simeq 2.4$ and $\simeq 3.3$ samples. Due to the large fraction of $z \simeq 6.2$ sources with $\log(M_{\rm BH}/M_\odot) \lesssim 8.5$, we can reject the hypothesis that the $M_{\rm BH}$ values at $z \simeq 4.8$ and $z \simeq 6.2$ are drawn from the same distribution.

Some of the above results may be biased by the fact that the four samples cover a different range of $L_{\rm bol}$, which originate from the different target selection criteria. We thus repeated the statistical tests aforementioned, focusing on subsamples which share a common range of $46.4 < \log\left(L_{\rm bol}/\text{erg s}^{-1}\right) < 47.4$ (i.e., matching the $L_{\rm bol}$ range of the $z \simeq 4.8$ sample). All but one comparison result in the same conclusions, with similar confidence levels. The one exception are the distributions of $M_{\rm BH}$ at $z \simeq 4.8$ and $z \simeq 6.2$, for which the null hypothesis now *cannot* be rejected, suggesting that these distributions represent the same parent population. This is not surprising given the lower luminosities of most of the $z \simeq 6.2$ sources, the dependence

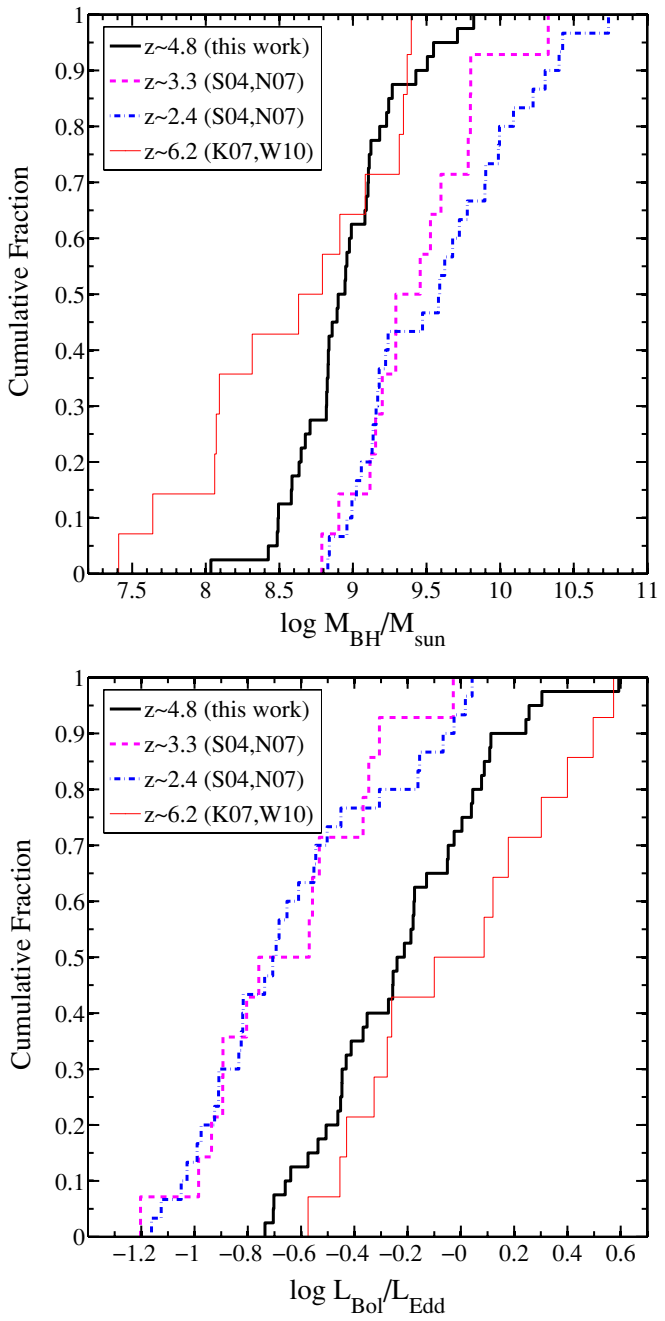

Figure 5. CDFs of $M_{\rm BH}$ (top) and $L/L_{\rm Edd}$ (bottom) for the samples discussed in the text.

(A color version of this figure is available in the online journal.)

of $M_{\rm BH}$ on source luminosity, and the incompleteness of the $z \simeq 6.2$ sample.

We conclude that there is strong evidence for a rise in $M_{\rm BH}$ and a drop in $L/L_{\rm Edd}$ of about a factor of 2.8 between $z \simeq 4.8$ and $z \simeq 3.3$. This strong trend is *not* observed with respect to neither lower nor higher redshift samples, which span similar periods of time.[6] It thus seems that the most massive BHs, associated with the most luminous AGNs, started the episode of fast BH growth at redshifts above $z \sim 5$. By $z \sim 2$–3, these SMBHs reach their peak (final) mass ($10^{10}\,M_{\odot}$) and their mass accretion is less efficient.

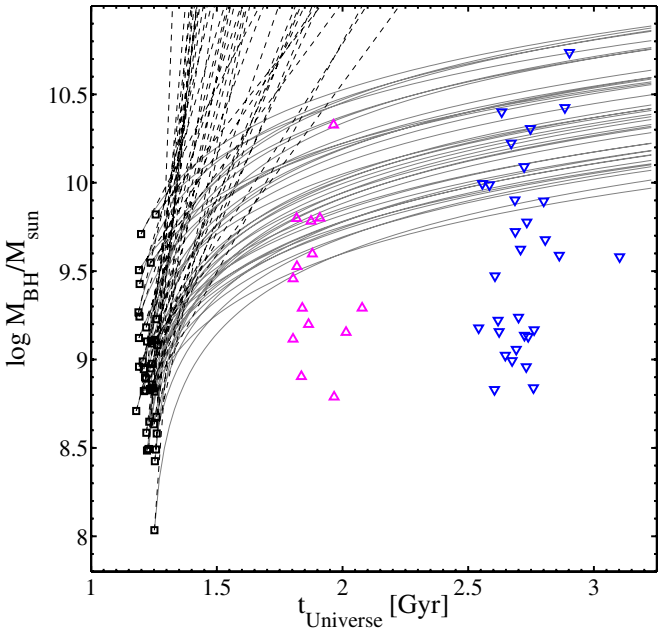

Figure 6. Evolution scenarios for the $z \simeq 4.8$ SMBHs. Symbols are identical to those in Figure 4. Solid lines describe the growth of $M_{\rm BH}$ under the assumption of a constant $L_{\rm bol}$, while dashed lines represent the constant $L/L_{\rm Edd}$ scenario.

(A color version of this figure is available in the online journal.)

5.2. The Growth of Active SMBHs from $z \simeq 4.8$ to $z \simeq 3.3$ and $z \simeq 2.4$

Given the trends and differences in $M_{\rm BH}$ and $L/L_{\rm Edd}$, as well as the short e-folding times of the $z \simeq 4.8$ AGNs (Section 4.2), it is possible to think of the $z \simeq 4.8$, $z \simeq 3.3$, and $z \simeq 2.4$ samples as representing different evolutionary stages of the same parent population of SMBHs. In what follows, we focus on the $z \simeq 4.8$ and $z \simeq 3.3$ samples (separated by ∼680 Myr) to test this evolutionary interpretation, assuming various scenarios.

We consider two growth scenarios: constant mass accretion rate (i.e., constant $L_{\rm bol}$) and constant $L/L_{\rm Edd}$.[7] As explained, the assumption of constant $L/L_{\rm Edd}$ results in an exponential growth of $M_{\rm BH}$ and given our chosen value of η, the mass growth e-folding time is $\tau \simeq 45\,(L/L_{\rm Edd})^{-1}$ Myr, which translates to $\tau \lesssim 240$ Myr ($L/L_{\rm Edd} > 0.18$) for the $z \simeq 4.8$ sources. Thus, even the lowest $L/L_{\rm Edd}$ SMBHs at $z \simeq 4.8$ could have increased their $M_{\rm BH}$ by a factor of ∼20 by $z \simeq 3.3$, which is much larger than the typical difference in $M_{\rm BH}$ between the two samples. The assumption of a constant $L_{\rm bol}$ results in much slower growth. The luminosities of the $z \simeq 4.8$ sources translate to $4\,M_{\odot}\,{\rm yr}^{-1} \lesssim \dot{M}_{\rm BH} \lesssim 37\,M_{\odot}\,{\rm yr}^{-1}$. Even this much slower growth scenario results in very high $M_{\rm BH}$ at $z \simeq 3.3$. This scenario also produces very low accretion rates ($L/L_{\rm Edd} < 0.1$) at $z \simeq 3.3$.

In Figure 6, we present evolutionary tracks for our $z \simeq 4.8$ AGNs to $z \simeq 3.3$ and eventually to $z = 2$. Clearly, continuous constant $L_{\rm bol}$ growth results in too large $M_{\rm BH}$ and cannot reproduce the lower $M_{\rm BH}$ sources at $z \simeq 2.4$ and $\simeq 3.3$. Specifically, the calculated distribution of $M_{\rm BH}$ for the $z \simeq 4.8$ sources, when evolved to $z \simeq 3.3$, has a median value of $\log(M_{\rm BH}/M_{\odot}) \simeq 10$, larger by ∼0.6 dex than the *observed* median of the $z \simeq 3.3$ sample. This scenario also fails to reproduce the observed range of $L/L_{\rm Edd}$, since the

[6] For the adopted cosmology, the physical time between $z = 4.8$ and $z = 3.3$ is ∼680 Myr and between $z = 3.3$ and $z = 2.4$ is ∼790 Myr.

[7] There are, of course, many other possible scenarios involving, for example, host-related evolution. These are beyond the scope of this paper.

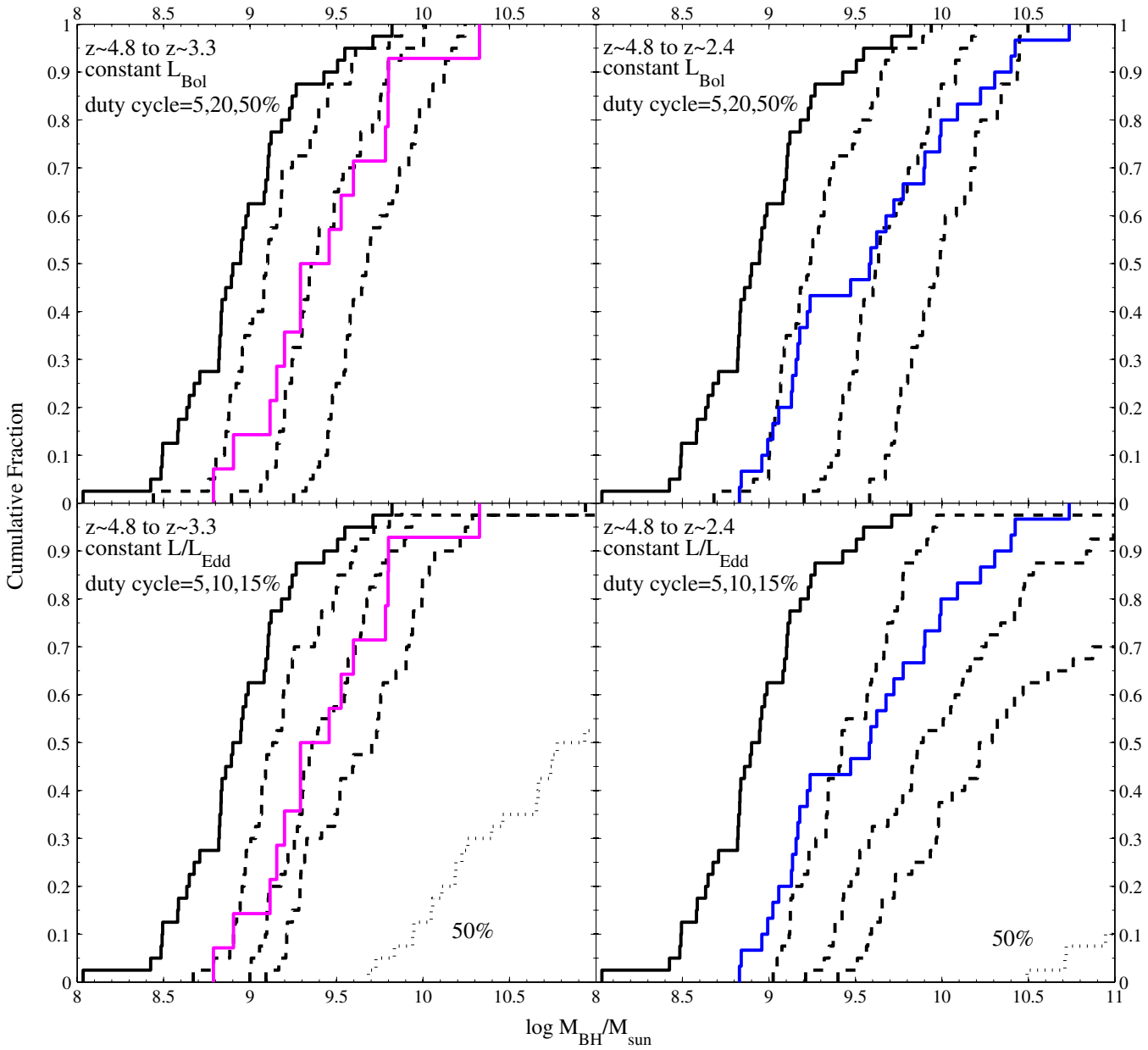

Figure 7. Observed and calculated $M_{\rm BH}$ CDFs for different evolutionary scenarios. In all panels, solid black lines show the observed $M_{\rm BH}$ CDF at $z \simeq 4.8$, while magenta lines (left panels) and blue lines (right panels) show the CDFs at $z \simeq 3.3$ and at $z \simeq 2.4$, respectively. Dashed black lines are the calculated CDF of the $z \simeq 4.8$ sample assuming different growth scenarios and duty cycles. Top panels assume a constant $L_{\rm bol}$ scenario, and duty cycles of 5%, 20%, and 50% (from left to right). Bottom panels assume a constant $L/L_{\rm Edd}$ scenario, and duty cycles of 5%, 10%, and 15% (from left to right). The dotted lines in the bottom panels illustrate how a duty cycle of 50% produces extremely overmassive BHs at $z \simeq 3.3$ and $z \simeq 2.4$. All the calculations assume $\eta = 0.1$. Assuming the extreme cases of $\eta = 0.05$ (or 0.3) would mean that the plotted calculated CDFs correspond to duty cycles which are a factor of $\sim$2 smaller (or larger; see the text for details).

lowest $L/L_{\rm Edd}$ sources at $z \simeq 3.3$ have $L/L_{\rm Edd} \gtrsim 0.1$. As the dotted evolutionary tracks in Figure 6 demonstrate, the constant $L/L_{\rm Edd}$ scenario produces even larger masses, and is only feasible if all the $z \simeq 4.8$ sources cease their accretion shortly after their observed active phase. This scenario assumes a constant $L/L_{\rm Edd}$, hence the significant difference between the $L/L_{\rm Edd}$ distributions at $z \simeq 4.8$ and at $z \simeq 3.3$ ($\sim$0.5 dex; see Figure 5) is not resolved. We also note that in both scenarios the $z \simeq 4.8$ sources would have been easily observed at $z \simeq 3.3$, since they would have $L_{\rm bol}$ which is either similar (linear growth) or much higher than (exponential growth) the sources observed by S04 and N07 at $z \simeq 2.4$ and $\simeq 3.3$. From these two simplistic growth scenarios, we conclude that the fast growth of the $z \simeq 4.8$ sources must either experience a shut down before $z \simeq 3.3$, or accrete in several short episodes, with duty cycles which are much smaller than unity.

To further constrain the evolution of the observed SMBHs, we ran a series of calculations with different duty cycles for each of the two evolutionary scenarios. In each calculation, we assembled the distribution of calculated $M_{\rm BH}$ at exactly $z = 3.3$ and $z = 2.4$. Several of these distributions are shown in Figure 7. For the fast, constant $L/L_{\rm Edd}$ scenario, the only calculated distributions which resemble the observed distribution of $M_{\rm BH}$ at $z \simeq 3.3$ are those with duty cycles in the range 7.5%–12.5%. The observed distribution at $z \simeq 2.4$, on the other hand, can only be achieved by duty cycles of 5%–7.5%. For the constant $L_{\rm bol}$ scenario, the $z \simeq 3.3$ distribution can be matched by assuming a duty cycle in the range of 15%–25%, while the

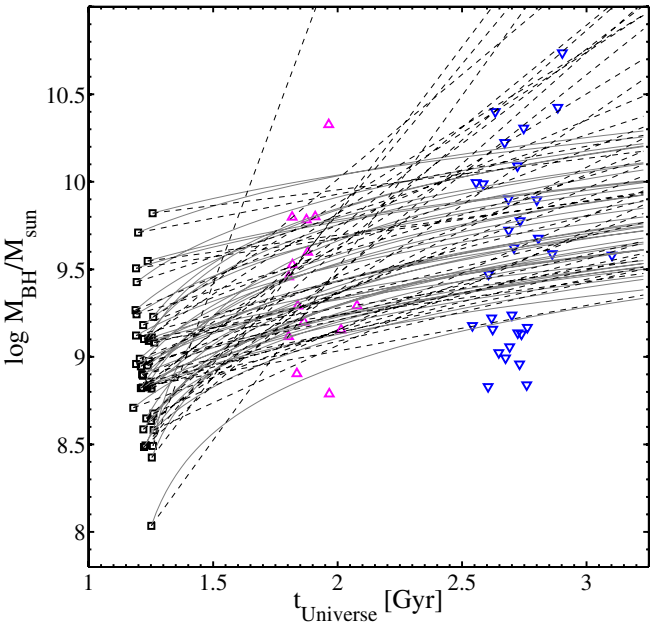

Figure 8. Evolution scenarios for the $z \simeq 4.8$ SMBHs with various duty cycles. Symbols are identical to those in Figure 4. Solid lines describe $M_{\rm BH}$ growth under the assumption of constant $L_{\rm bol}$ and a duty cycle of 20%. Dashed lines represent the constant $L/L_{\rm Edd}$ scenario and a duty cycle of 10%.

(A color version of this figure is available in the online journal.)

$z \simeq 2.4$ distributions can be partially explained by assuming duty cycles of ∼5%–25%. The ranges of duty cycles which account for the observed distribution of $L/L_{\rm Edd}$ are somewhat different: 10%–15% for the $L/L_{\rm Edd}$ distribution at $z \simeq 3.3$ and 5%–10% for the one at $z \simeq 2.4$. All the above calculations assumed $\eta = 0.1$. Naturally, lower (higher) radiative efficiencies will require shorter (longer) duty cycles to reproduce the same calculated CDFs at $z \simeq 2.4$ and $\simeq 3.3$. This means that for any assumed η in the range $0.05 \leqslant \eta \leqslant 0.3$ the aforementioned "acceptable" duty cycles can change by up to a factor of ∼2, where the exact factor scales as $\eta/(1-\eta)$. We note that Figure 7 suggests that, in both evolution scenarios, the more massive BHs at $z \simeq 2.4$ and $\simeq 3.3$ seem to have grown at higher duty cycles than the less massive ones. Alternatively, this can be interpreted as an increase in radiative efficiency with increasing resultant $M_{\rm BH}$ at $z \simeq 2.4$ and $\simeq 3.3$. In particular, the observed distributions of $M_{\rm BH}$ and $L/L_{\rm Edd}$ at $z \simeq 2.4$ are much more complex than the calculated ones and no single, fixed duty cycle can account for the shape of the observed distributions. The reason for this apparent discrepancy might also be the way the $z \simeq 2.4$ sources were selected in the S04 and N07 studies.

To illustrate how the above duty cycles facilitate an evolutionary connection between the three samples, we present in Figure 8 the evolutionary tracks of the $z \simeq 4.8$ sample, similar to Figure 6, but this time assuming duty cycles of 10% and 20%, for the constant $L/L_{\rm Edd}$ and constant $L_{\rm bol}$ scenarios, respectively, and assuming again $\eta = 0.1$. We also verified that evolving the $M_{\rm BH}$ of the $z \simeq 2.4$ and $\simeq 3.3$ sources *backwards*, under the assumption of constant $L/L_{\rm Edd}$ and a duty cycle of 10% results in a distribution of $M_{\rm BH}$ which is not critically different than the one directly observed at $z \simeq 4.8$. However, we again find that the few highest $M_{\rm BH}$ sources at $z \simeq 2.4$ probably require higher duty cycles.

We conclude that all the observed measurements of $M_{\rm BH}$, $L/L_{\rm Edd}$, and $L_{\rm bol}$ are consistent with duty cycles of about 10% –20%. Considerably longer duty cycles can be consistent with observations only if we assume an extremely high radiative efficiency ($\eta \simeq 0.3$) for all the $z \simeq 4.8$ sources. Such low duty cycles are in good agreement with the models presented in Shankar et al. (2009), which are able to reproduce the growth of a similar population of SMBHs, in terms of redshift and range of $M_{\rm BH}$ (see their Figure 7). Our constrains on duty cycles are, however, in contrast with several other studies that suggest that the duty cycle at high redshift should reach unity, based on the clustering of high-redshift AGNs (e.g., White et al. 2008; Wyithe & Loeb 2009; Bonoli et al. 2010; and references therein).

All this leads us to suggest that for the most massive $z > 2$ type-I AGNs, an epoch of fast SMBH growth took place before $z \sim 4$, which we partially observe at $z \simeq 4.8$. This epoch is efficient enough to produce the very massive ($\log(M_{\rm BH}/M_\odot) \gtrsim 10$) BHs observed at $z \simeq 2.4$. The fast growth slows down before $z \simeq 3.3$, and the sources observed at $z \simeq 3.3$ show much lower $L/L_{\rm Edd}$. In addition, there is no significant rise in $M_{\rm BH}$ between $z \simeq 3.3$ and $z \simeq 2.4$. The growth of $M_{\rm BH}$ during this epoch can only be explained by assuming that mass accretion proceeded in short episodes, lasting an order 10%–20% of the total period. This translates to accretion episodes which cumulatively last ∼70–140 Myr (∼150–300 Myr) over the period between $z \simeq 4.8$ and $z \simeq 3.3$ ($z \simeq 4.8$ and $z \simeq 2.4$), respectively. Another possibility is that the $z \simeq 4.8$ SMBHs have experienced an even faster shut down, and so at $z \simeq 3.3$ their inactive relics have masses that do not differ significantly from those we observe at $z \simeq 4.8$.

Major mergers between massive, gas-rich galaxies are capable of supplying large amounts of cold gas directly to the innermost regions to be accreted by the central SMBHs. Detailed simulations of such mergers suggest that these events can fuel significant BH growth over periods of ∼1 Gyr. The mass accretion rate and source luminosity during such mergers may vary on timescales of few × 10 Myr (Di Matteo et al. 2005; Hopkins et al. 2006; Hopkins & Hernquist 2009). According to Hopkins et al. (2006), AGNs would appear to have $L_{\rm bol} \gtrsim 2.7 \times 10^{46}$ erg s^{-1} (i.e., matching the range we observe at $z \simeq 4.8$) for typically $\lesssim$ 100 Myr. Numerical studies suggest that massive dark matter halos may undergo more than one major merger per Gyr at $z \simeq 4.8$ (e.g., Genel et al. 2009 and references therein). Thus, during the ∼680 Myr between $z \simeq 4.8$ and $z \simeq 3.3$, the hosts of the $z \simeq 4.8$ SMBHs may have undergone a single merger, during which the period of significant accretion by the SMBHs would last for $\lesssim$100 Myr. This is in good agreement with the duty cycles of 10%–20% we find here, which correspond to 70–140 Myr. The decline in activity observed for the most massive BHs at $z \simeq 3.3$ and $z \simeq 2.4$ may then be associated with the decline in the major merger rate, which drops by a factor of ∼4 between $z \simeq 4.8$ and $z \simeq 2.4$ (Genel et al. 2009). However, it is likely that the hosts of the $z \simeq 2.4$ SMBHs have experienced an additional major merger during the ∼790 Myr between $z \simeq 3.3$ and $z \simeq 2.4$, especially if these SMBHs reside in the more massive dark matter halos. In such a scenario, the largest BHs at $z \simeq 2.4$ may have gathered their high mass during more efficient (i.e., higher duty cycle) accretion episodes. This requirement of higher duty cycles for higher $M_{\rm BH}$ sources is also reflected in our analysis (see upper right panel of Figure 7). If major mergers are indeed the main drivers of SMBH accretion history at $z \sim 2$–5, the results presented here predict that the host galaxies of the $z \simeq 4.8$ sources would be found in the early stages of major mergers, while the hosts of $z \simeq 2.4$ and $\simeq 3.3$ sources would appear to be in either later stages, or in merging systems which have a lower mass ratio.

There are several other mechanisms to make large amounts of cold gas available for BH accretion. Most of these might also trigger intense star formation (SF) activity in the hosts of SMBHs. Indeed, many high-luminosity AGNs show evidence for intense SF (e.g., Netzer 2009b; Lutz et al. 2010, and references therein). New observations by *Herschel* suggest that SF in the hosts of the most luminous AGN peaks at $z \sim 3$ and quickly decreases at later epochs (Serjeant et al. 2010). If correct, it will indicate that the amount of gas available for both BH accretion and SF has depleted by $z \sim 2$–3, consistent with the decrease in SMBH accretion activity we find here. Future *Herschel* and ALMA observations of the hosts of the $z \simeq 4.8$ AGNs may be able to reveal the presence of such SF activity, and perhaps the amount and dynamical state of the cold gas. This will enable a better understanding of the galaxy-scale processes which drive the accretion history of the fast-growing $z \simeq 4.8$ SMBHs.

6. SUMMARY

We present new *H*-band spectroscopy for a flux-limited sample of 40 type-I SDSS AGNs at $z \simeq 4.8$. The sample covers $\sim$1/4 of all the (spectroscopically observed) SDSS sources at that redshift band, and thus about $\sim$1/20 of the total population of $L_{\rm bol} > 2.75 \times 10^{46}$ erg s^{-1} sources (over the entire sky). The main results of our study are as follows.

1. The $z \simeq 4.8$ AGNs have, on average, higher accretion rates and lower masses than those observed at lower redshifts. The accretion rates and masses are comparable to those of the small, incomplete samples of $z \simeq 6.2$ AGNs.
2. We have observed an epoch of fast SMBH growth, probably the very first such phase for most SMBHs. Assuming continuous growth from about $z = 20$, these observations provide the very first look at the distribution of seed BHs in the early universe. About 65% of the SMBHs at $z \simeq 4.8$ have had enough time to grow to their observed $M_{\rm BH}$, assuming continuous accretion at the observed $L/L_{\rm Edd}$. About 40% of the sources could have started their growth from BH seeds which are stellar remnants ($M_{\rm seed} < 100\,M_{\odot}$). For the minority the sources, those with small $L/L_{\rm Edd}$, there might have been an even earlier epoch of faster accretion or, perhaps, they started their growth from much larger seeds ($M_{\rm seed} \gtrsim 10^6\,M_{\odot}$).
3. The $z \simeq 4.8$ sources can be regarded as the progenitor population of the most massive ($M_{\rm BH} \gtrsim 10^{10}\,M_{\odot}$) BHs observed at $z \simeq 2.4$ and $\simeq 3.3$. The growth rate of those massive BHs seems to be much slower between $z \simeq 3.3$ and $z \simeq 2.4$.
4. A comparison of the observed distributions of $M_{\rm BH}$ at $z \simeq 4.8$, $z \simeq 3.3$, and $z \simeq 2.4$ indicates that the $z \simeq 4.8$ sources either completely stop their accretion shortly after $z \simeq 4.8$, or that their accretion proceeds in relatively short episodes. We find that for mass growth rates which follow either constant $L/L_{\rm Edd}$ or constant $L_{\rm bol}$ scenarios, duty cycles of either $\sim$10% or $\sim$20%, respectively, give reasonable agreement to the observed distributions of $M_{\rm BH}$.

We thank the referee for his/her detailed comments and suggestions. We also thank Richard Davies for his patient help with SINFONI data reduction.

Funding for this work has been provided by the Israel Science Foundation grant 364/07 and by the Jack Adler Chair for Extragalactic Astronomy. B.T. acknowledges generous support by the Dan David Foundation. P.L. thanks support by Fondecyt project No. 1080603.

This work is based on observations collected at the European Organization for Astronomical Research in the Southern Hemisphere, Chile, and in addition on observations obtained at the Gemini Observatory, which is operated by the Association of Universities for Research in Astronomy, Inc., under a cooperative agreement with the NSF on behalf of the Gemini partnership: the National Science Foundation (United States), the Science and Technology Facilities Council (United Kingdom), the National Research Council (Canada), CONICYT (Chile), the Australian Research Council (Australia), Ministério da Ciência e Tecnologia (Brazil) and the Ministerio de Ciencia, Tecnología e Innovación Productiva (Argentina)

This work makes use of data from the SDSS. Funding for the SDSS and SDSS-II has been provided by the Alfred P. Sloan Foundation, the Participating Institutions, the National Science Foundation, the US Department of Energy, the National Aeronautics and Space Administration, the Japanese Monbukagakusho, the Max Planck Society, and the Higher Education Funding Council for England. The SDSS Web Site is http://www.sdss.org/.

REFERENCES

Adelman-McCarthy, J. K., et al. 2008, ApJS, 175, 297
Baldwin, J. A., Ferland, G. J., Korista, K. T., Hamann, F., & LaCluyzé, A. 2004, ApJ, 615, 610
Baskin, A., & Laor, A. 2005, MNRAS, 356, 1029
Bauer, A., Baltay, C., Coppi, P., Ellman, N., Jerke, J., Rabinowitz, D., & Scalzo, R. 2009, ApJ, 696, 1241
Becker, R. H., White, R. L., & Helfand, D. J. 1995, ApJ, 450, 559
Begelman, M. C., Volonteri, M., & Rees, M. J. 2006, MNRAS, 370, 289
Bentz, M. C., Peterson, B. M., Netzer, H., Pogge, R. W., & Vestergaard, M. 2009, ApJ, 697, 160
Bonoli, S., Shankar, F., White, S. D. M., Springel, V., & Wyithe, J. S. B. 2010, MNRAS, 404, 399
Corbett, E. A., et al. 2003, MNRAS, 343, 705
Croom, S. M., et al. 2009, MNRAS, 399, 1755
Cutri, R. M., et al. 2003, The IRSA 2MASS All-Sky Point Source Catalog, NASA/IPAC Infrared Science Archive, http://irsa.ipac.caltech.edu/applications/Gator/
Davies, R. I. 2007, MNRAS, 375, 1099
Devecchi, B., & Volonteri, M. 2009, ApJ, 694, 302
Di Matteo, T., Springel, V., & Hernquist, L. 2005, Nature, 433, 604
Eisenhauer, F., et al. 2003, Proc. SPIE, 4841, 1548
Elvis, M., et al. 1994, ApJS, 95, 1
Fan, X., et al. 2006, AJ, 132, 117
Fine, S., Croom, S. M., Bland-Hawthorn, J., Pimbblet, K. A., Ross, N. P., Schneider, D. P., & Shanks, T. 2010, MNRAS, 409, 591
Fine, S., et al. 2008, MNRAS, 390, 1413
Genel, S., Genzel, R., Bouché, N., Naab, T., & Sternberg, A. 2009, ApJ, 701, 2002
Hasinger, G., Miyaji, T., & Schmidt, M. 2005, A&A, 441, 417
Heger, A., & Woosley, S. E. 2002, ApJ, 567, 532
Hodapp, K. W., et al. 2003, PASP, 115, 1388
Hopkins, P. F., & Hernquist, L. 2009, ApJ, 698, 1550
Hopkins, P. F., Hernquist, L., Cox, T. J., Di Matteo, T., Robertson, B., & Springel, V. 2006, ApJS, 163, 1
Kaspi, S., Maoz, D., Netzer, H., Peterson, B. M., Vestergaard, M., & Jannuzi, B. T. 2005, ApJ, 629, 61
Kaspi, S., Smith, P. S., Netzer, H., Maoz, D., Jannuzi, B. T., & Giveon, U. 2000, ApJ, 533, 631
Kellermann, K. I., Sramek, R., Schmidt, M., Shaffer, D. B., & Green, R. 1989, AJ, 98, 1195
King, A. 2008, New Astron. Rev., 52, 253
King, A. R., Pringle, J. E., & Hofmann, J. A. 2008, MNRAS, 385, 1621
Kurk, J. D., et al. 2007, ApJ, 669, 32
Kurosawa, R., & Proga, D. 2009, MNRAS, 397, 1791
Lawrence, A., et al. 2007, MNRAS, 379, 1599
Lutz, D., et al. 2010, ApJ, 712, 1287

Marconi, A., Axon, D. J., Maiolino, R., Nagao, T., Pastorini, G., Pietrini, P., Robinson, A., & Torricelli, G. 2008, ApJ, 678, 693
Marconi, A., Risaliti, G., Gilli, R., Hunt, L. K., Maiolino, R., & Salvati, M. 2004, MNRAS, 351, 169
Marziani, P., Sulentic, J. W., Stirpe, G. M., Zamfir, S., & Calvani, M. 2009, A&A, 495, 83
McLure, R. J., & Dunlop, J. S. 2004, MNRAS, 352, 1390
McLure, R. J., & Jarvis, M. J. 2004, MNRAS, 353, L45
Merloni, A. 2004, MNRAS, 353, 1035
Mineshige, S., Kawaguchi, T., Takeuchi, M., & Hayashida, K. 2000, PASJ, 52, 499
Miyaji, T., Hasinger, G., & Schmidt, M. 2001, A&A, 369, 49
Netzer, H. 2009a, ApJ, 695, 793
Netzer, H. 2009b, MNRAS, 399, 1907
Netzer, H., & Marziani, P. 2010, ApJ, 724, 318
Netzer, H., & Trakhtenbrot, B. 2007, ApJ, 654, 754
Netzer, H., Lira, P., Trakhtenbrot, B., Shemmer, O., & Cury, I. 2007, ApJ, 671, 1256 (N07)
Richards, G. T., et al. 2006a, AJ, 131, 2766
Richards, G. T., et al. 2006b, ApJS, 166, 470
Salviander, S., Shields, G. A., Gebhardt, K., & Bonning, E. W. 2007, ApJ, 662, 131
Serjeant, S., et al. 2010, A&A, 518, L7
Shankar, F. 2009, New Astron. Rev., 53, 57
Shankar, F., Crocce, M., Miralda-Escudé, J., Fosalba, P., & Weinberg, D. H. 2010a, ApJ, 718, 231
Shankar, F., Salucci, P., Granato, G. L., De Zotti, G., & Danese, L. 2004, MNRAS, 354, 1020
Shankar, F., Sivakoff, G. R., Vestergaard, M., & Dai, X. 2010b, MNRAS, 401, 1869
Shankar, F., Weinberg, D. H., & Miralda-Escudé, J. 2009, ApJ, 690, 20
Shemmer, O., Netzer, H., Maiolino, R., Oliva, E., Croom, S., Corbett, E., & di Fabrizio, L. 2004, ApJ, 614, 547 (S04)
Shen, Y., Greene, J. E., Strauss, M. A., Richards, G. T., & Schneider, D. P. 2008, ApJ, 680, 169
Shen, Y., et al. 2007, AJ, 133, 2222
Shen, Y., et al. 2010, ApJ, 719, 1693
Sigut, T. A. A., & Pradhan, A. K. 2003, ApJS, 145, 15
Sijacki, D., Springel, V., Di Matteo, T., & Hernquist, L. 2007, MNRAS, 380, 877
Silverman, J. D., et al. 2008, ApJ, 679, 118
Soltan, A. 1982, MNRAS, 200, 115
Vanden Berk, D. E., et al. 2001, AJ, 122, 549
van der Bliek, N. S., et al. 2004, Proc. SPIE, 5492, 1582
Vestergaard, M., & Peterson, B. M. 2006, ApJ, 641, 689
Vestergaard, M., & Wilkes, B. J. 2001, ApJS, 134, 1
Volonteri, M. 2010, A&ARv, 18, 279
Volonteri, M., Haardt, F., & Madau, P. 2003, ApJ, 582, 559
Volonteri, M., Madau, P., Quataert, E., & Rees, M. J. 2005, ApJ, 620, 69
Wang, J.-M., & Netzer, H. 2003, A&A, 398, 927
Wang, J.-M., et al. 2009, ApJ, 697, L141
White, R. L., Becker, R. H., Helfand, D. J., & Gregg, M. D. 1997, ApJ, 475, 479
White, M., Martini, P., & Cohn, J. D. 2008, MNRAS, 390, 1179
Willott, C. J., et al. 2010, AJ, 140, 546
Woo, J.-H., & Urry, C. M. 2002, ApJ, 581, L5
Wyithe, J. S. B., & Loeb, A. 2009, MNRAS, 395, 1607
York, D. G., et al. 2000, AJ, 120, 1579